

Stratigraphic architecture, magnetostratigraphy, and incised-valley systems of the Pliocene-Pleistocene collisional marine foreland basin of Taiwan

Wen-Shan Chen

Department of Geology, National Taiwan University, 245 Choushan Road, Taipei, Taiwan, Republic of China

Kenneth D. Ridgway*

Department of Earth and Atmospheric Sciences, Purdue University, West Lafayette, Indiana 47907-1397, USA

Chorng-Shern Horng

Institute of Earth Sciences, Academia Sinica, Taipei, Taiwan, Republic of China

Yue-Gau Chen

Department of Geology, National Taiwan University, 245 Choushan Road, Taipei, Taiwan, Republic of China

Kai-Shuan Shea

Central Geological Survey, Ministry of Economic Affairs, Taipei, Taiwan, Republic of China

Ming-Guan Yeh

Taiwan Petroleum Exploration Division, Chinese Petroleum Corporation, P.O. Box 63, Miaoli, Taiwan, Republic of China

ABSTRACT

Lithofacies analysis, magnetostratigraphy, and seismic profiles of Pliocene-Pleistocene foreland basin deposits of Taiwan provide a framework to evaluate the stratigraphic development of a collisional marine foreland basin. We have recognized several scales of stratigraphic packages and unconformities in deposits of the Taiwan foreland basin. Small-scale (20 to 150 m thick) stratigraphic sequences contain upward-shallowing, marine lithofacies successions that are bracketed by thin coquina sandstones. We interpret the small-scale stratigraphic packages as "parasequences" in the traditional sequence stratigraphy model, the thin coquina sandstones representing marine-flooding intervals. The average duration of individual small-scale packages was in the range of 37.5 k.y., on the basis of our magnetostratigraphy. These sequences are interpreted as the product of eustatic sea-level change possibly related to the orbital time series of obliquity.

Intermediate-scale stratigraphic sequences are 150 to 1000 m thick and are bounded

by unconformities that are well exposed in outcrop and can be clearly identified in seismic sections. The unconformity surfaces have several hundred meters of relief and represent periods of major fluvial valley incision in the foreland basin. One of the unconformities is locally an angular one that we interpret as representing a growth structure that formed during structural uplift of the proximal margin of the foreland basin at ca. 1.25 Ma. Across this angular unconformity, there were marked increases in rates of sediment accumulation and tectonic subsidence in the foreland basin. Other major unconformities that bound intermediate-scale stratigraphic sequences are high-relief disconformities. These unconformities may be the product of eustatic changes, because there has been little change in rates of sediment accumulation and tectonic subsidence across these unconformities. The duration of individual, intermediate-scale packages ranges from ~100 000 to 700 000 yr, on the basis of magnetostratigraphy and biostratigraphy. We interpret the intermediate-scale sequences as "sequences" in the traditional sequence stratigraphy model.

Our analysis of the Pliocene-Pleistocene

deposits of the Taiwan foreland basin has several implications for understanding the stratigraphic evolution of this collisional marine foreland basin. (1) Deposition in the Taiwan foreland basin appears to have been punctuated by at least five episodes of erosion and major fluvial valley incision. Large volumes of sediment were eroded from the proximal margin of the foreland basin and transported to more distal parts of the foreland basin or to depocenters outside the foreland basin system during all stages of basin development. (2) The presence of high-relief unconformities and growth structures in the Pliocene-Pleistocene foreland basin deposits suggests a well-developed wedge-top depozone in the foreland basin system. (3) The Pliocene-Pleistocene strata of the foreland basin of Taiwan record ~2.3 m.y. of deposition, on the basis of our magnetostratigraphy. Sediment accumulation rate was on the order of ~950 m/m.y. during the earlier stages of basin development. During the later stages of basin development, sediment accumulation rate increased to ~1900 m/m.y. Sediment accumulation rates in the collisional marine foreland basin of Taiwan are much higher than previously published rates

*Corresponding author; e-mail: ridge@purdue.edu.

from more extensively studied retroarc foreland basins and collisional nonmarine foreland basins.

Keywords: foreland basin, magnetostratigraphy, Pliocene-Pleistocene, Taiwan, unconformities.

INTRODUCTION

A fundamental problem in interpreting the stratigraphic record of foreland basins is understanding the relative roles of eustasy, tectonics, and sediment supply (Jordan, 1995; Miall, 1995). Analysis of the Pliocene-Pleistocene foreland basin of Taiwan has much to offer on this problem because it contains a 3–5-km-thick section of well-exposed strata that were deposited not only in a well-studied active tectonic setting (Covey, 1984, 1986; Teng, 1987; Suppe, 1988; among others) but also during a relatively recent interval when eustatic variations are fairly well understood from the oxygen isotope record of deep-sea cores (Shackleton et al., 1995a). This basin is the result of the oblique collision of the Luzon volcanic arc with the southeastern continental margin of China (Fig. 1A; Chai, 1972; Ho, 1982; Teng, 1990). Oblique arc–continent collision has resulted in the progressive migration of active deformation and foreland basin development from north to south (Suppe, 1981; Covey, 1984). In response to oblique collision, the Taiwan foreland basin has been filled axially with nearshore and nonmarine deposystems predominantly in the north and with offshore marine deposystems predominantly in the south (Covey, 1984). This paper presents a study of the Pliocene-Pleistocene deposits utilizing lithofacies analysis, magnetostratigraphy, and seismic data to evaluate eustatic, tectonic, and sediment-supply controls on deposition in the foreland basin. Seven detailed measured stratigraphic sections, along a north-south traverse of the foreland basin (Figs. 1B, 2), provide the framework for our analysis. We present stratigraphic and sedimentologic data in this paper from the two best exposed and most continuous measured

sections. One section, from south-central Taiwan (Chengwenchi section in Figs. 1B, 2), is ~2400 m thick and characterizes the offshore marine deposits of the Pliocene-Pleistocene foreland basin. A second, ~3440-m-thick section from north-central Taiwan (Tsaohuchi section in Figs. 1B, 2) contains a larger percentage of nearshore and nonmarine deposits of the foreland basin. Age control for the two sections is based on magnetostratigraphic and biostratigraphic data.

An important finding from our study is the recognition of high-relief unconformities and growth structures in Pliocene-Pleistocene deposits along the proximal side of the foreland basin, implying that much of the stratigraphic record has been eroded. The new magnetostratigraphy also allows us to address rates of sediment accumulation and tectonic subsidence in this collisional marine foreland basin.

GEOLOGIC SETTING

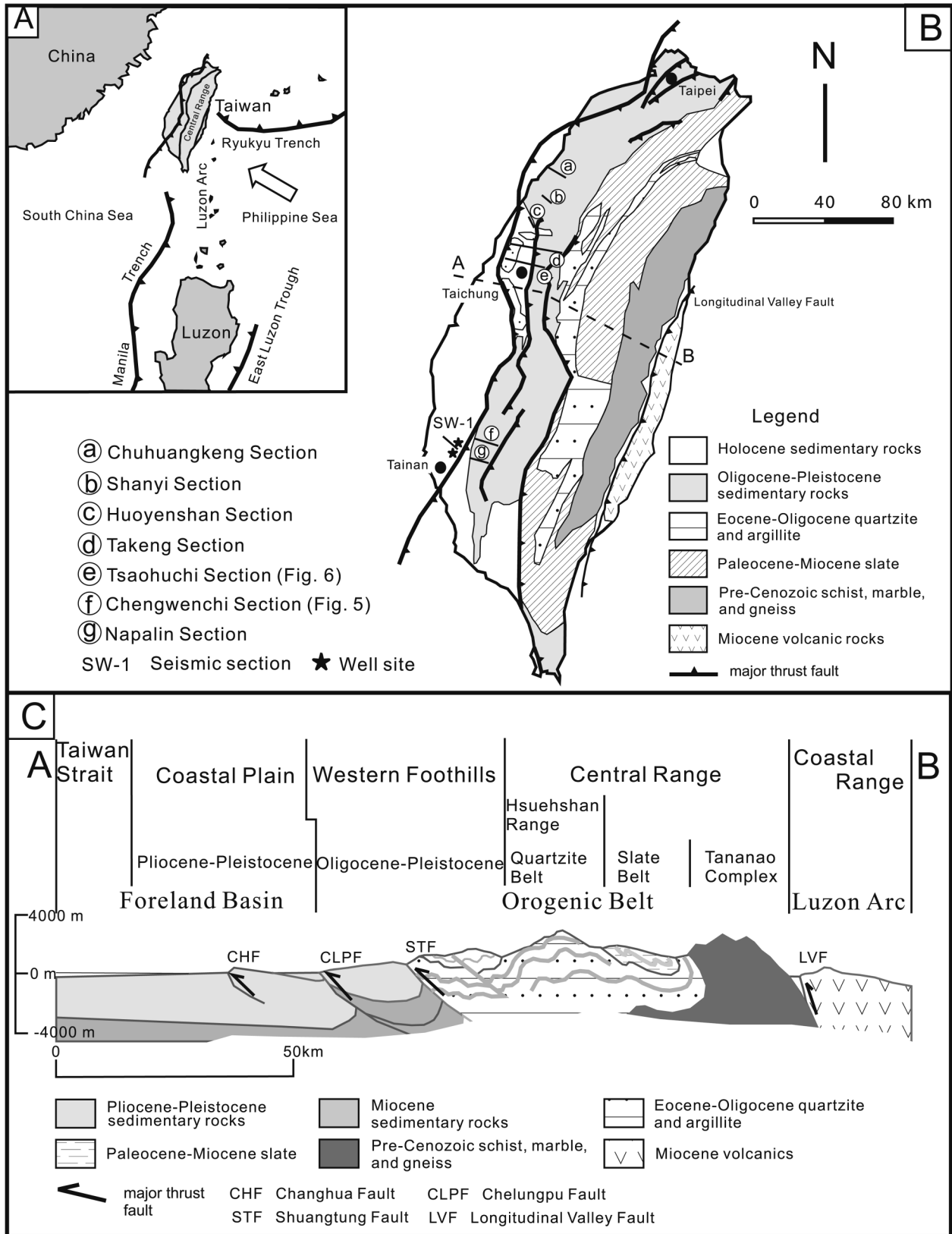
Taiwan represents the subaerial part of an active orogenic belt that is forming as a result of the collision of the Luzon volcanic arc with the southeastern passive margin of China (Fig. 1A; Chai, 1972). Oblique arc–continent collision began during the late Miocene (Chen et al., 1985; Sung and Wang, 1985; Hsieh, 1990) and has resulted in progressive migration of active deformation and foreland basin development from north to south (Suppe, 1981; Lacombe et al., 1999). Inception of mountain building of the Central Range (Fig. 1C), for example, began at ca. 6–5 Ma in northern Taiwan and at ca. 3 Ma in central Taiwan, on the basis of zircon fission-track ages (Hsieh, 1990). Today, the collision is propagating southward at a rate of 5.5 cm/yr (Byrne and Crespi, 1997). Southward propagation of active deformation and foreland basin development has resulted in a southward fining of lithofacies in the basin. The northern part of the foreland basin is dominated by shallow marine and nonmarine deposits, whereas the southern part of the foreland basin is dominated by deeper marine deposits (Covey, 1984, 1986; Teng, 1987).

The geology of Taiwan can be divided into four major tectonostratigraphic elements: the Coastal Plain, the Western Foothills, the Central Range, and the Coastal Range (Fig. 1C; Ho, 1986). The Pliocene-Pleistocene foreland basin deposits that we studied are located in the Coastal Plain and Western Foothills (Fig. 1, B and C). The active foreland basin represents a major zone of subsidence dynamically linked to the adjacent orogenic belt since the late Pliocene (Covey, 1986; Teng, 1987). The eastern margin of the foreland basin is defined by a series of imbricate thrust faults that have incorporated foreland basin deposits into a series of thrust sheets that form the Western Foothills (Fig. 1, B and C; Ho, 1976; Suppe, 1980; Angelier et al., 1986; Hung and Wiltshko, 1993; Lee et al., 1996; Mouthereau et al., 1999). The strata carried in these thrust sheets provide several well-exposed, complete sections of the Pliocene-Pleistocene foreland basin deposits (Fig. 2). In north-central Taiwan, Pliocene-Pleistocene deposits consist mainly of the Cholan Formation and the Toukoshan Formation (Fig. 2). The Toukoshan Formation is divided into a lower sandstone-dominated unit, the Hsiangshan Member, and an upper conglomerate-dominated unit, the Huoyenshan Member (Fig. 2). In south-central Taiwan, there are several local stratigraphic names for the Pliocene-Pleistocene deposits. In this article, we use the stratigraphic names designed for the Chengwenchi area; they are, from oldest to youngest, the Yunshuichi, Liuchungchi, Kanhsialiao, Erhchungchi, and Liushuang Formations (Fig. 2).

PALEOMAGNETIC DATA

In order to establish a chronologic framework for the Pliocene-Pleistocene foreland basin deposits, we sampled the Chengwenchi and Tsaohuchi measured sections (sections f and e in Fig. 1B) for magnetostratigraphic analysis. Paleomagnetic sampling focused on fine-grained deposits because they generally favor preservation of reliable magnetic signals. At each site, cores (25 mm in diameter) were drilled, after removing the weathering

Figure 1. (A) Regional map showing the major tectonic elements of the Taiwan region. Taiwan is located along the convergent boundary between the Philippine Sea plate and the continental margin of China. (B) Major geologic elements of Taiwan. Circled letters show location of our measured stratigraphic sections. The Chengwenchi section, near the city of Tainan (black circle) in south-central Taiwan, is shown in Figure 5. The Tsaohuchi section, located near the city of Taichung (black circle) in north-central Taiwan, is shown in Figure 6. SW-1 is the line of seismic section shown in Figure 10. Stars near the seismic line represent locations of two petroleum wells that provide biostratigraphic data and geophysical well logs used for interpretation of the seismic line. Dashed line A–B shows the location of the cross section in C. Geology modified from Ho (1986). (C) Schematic cross section of central Taiwan showing major tectonic elements. See B for location of line of cross section. Geology from Ho (1986, 1988).



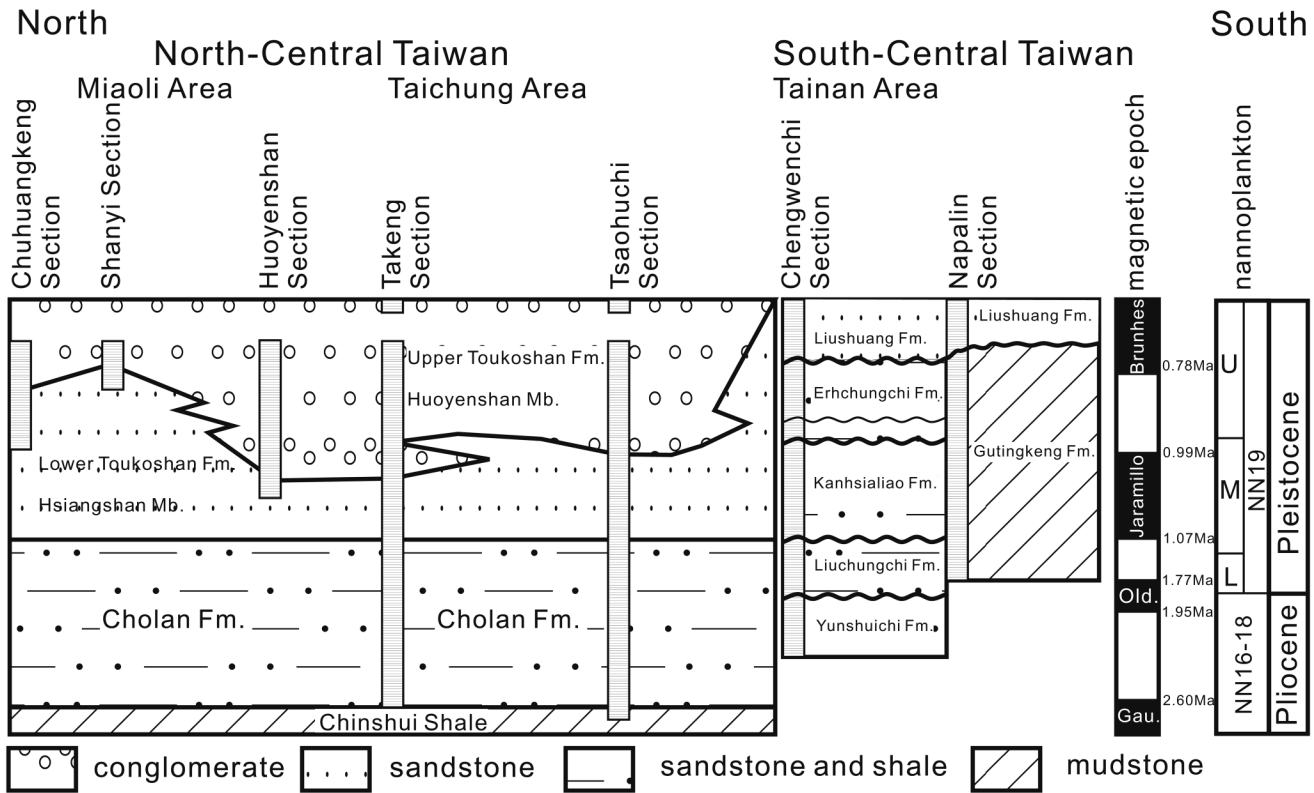


Figure 2. North-south stratigraphic cross section through the foreland basin of western Taiwan. Columns represent our measured stratigraphic sections. Nannoplankton zonation from Martini (1971). Magnetostratigraphic age control is from our analysis of the Tsaohuchi and Chengwenchi measured sections. See Figure 1B for geographic locations of measured sections. Note that the horizontal distance between measured sections is not to scale.

surface of the outcrop, and were oriented (i.e., azimuth and dip) with a mechanical device mounted with a magnetic compass. Bedding attitude was also measured at each site for structural correction. A total of 184 and 40 sites were obtained from the Chengwenchi and Tsaohuchi sections, respectively. Sites were spaced at stratigraphic intervals of 5 to 60 m, depending on lithology and exposure.

Samples 22 mm long were cut from the oriented cores and were analyzed for natural remanent magnetization (NRM) with a 2G Enterprises superconducting rock magnetometer. Thermal demagnetization was conducted with an ASC thermal demagnetizer that has a low-field (<10 nT) cooling chamber. The magnetometer and thermal demagnetizer were both situated in a magnetically shielded room. More than eight steps from room temperature to 360 or 400 °C were employed. As shown in Figure 3, this temperature range is sufficient to clean the secondary remanent component of NRM and reveal a characteristic remanent magnetization (ChRM) for magnetic polarity determination. Using the line-fitting vector components (Kirschvink, 1980), we calculated

the mean directions of the ChRMs of samples and then constructed a magnetostratigraphy for the studied sections (Fig. 4).

LITHOFACIES DATA

Figures 5 and 6 are logs of the Chengwenchi and Tsaohuchi measured stratigraphic sections showing lithofacies data and magnetostratigraphy. The Chengwenchi section is representative of offshore marine deposits of the distal foreland basin, whereas the Tsaohuchi section is more representative of nearshore and nonmarine deposits of the proximal part of the foreland basin. We recognize small-scale, intermediate-scale, and large-scale stratigraphic packages in the foreland basin deposits. The sedimentological details of our measured sections are summarized in Figures 5 and 6. Figure 2 shows our lithofacies correlation between measured stratigraphic sections and their correlation to the magnetostratigraphic framework (Fig. 4) and previously published biostratigraphy (Chen et al., 1977; Chi, 1978; Chang and Chi, 1983; Horng, 1991).

Small-Scale Stratigraphic Packages

South-Central Taiwan: Distal Foreland Basin Strata

Common small-scale stratigraphic sequences recognized in south-central Taiwan consist of three dominant lithofacies: a lower mudstone-dominated one with a basal coquina sandstone, a middle lithofacies of sandstone interbedded with mudstone, and an upper sandstone-dominated lithofacies. The small-scale sequences typically range in thickness from 20 to 50 m and are extremely well developed in the Yunshuichi and Liuchungchi Formations (0 to 640 m in Fig. 5). Thicker small-scale sequences, on the order of 150 m, are common in the Kanhsialiao, Erchungchi, and Liushuang Formations (640 m to 2400 m in Fig. 5).

The lower lithofacies of these small-scale sequences consists predominantly of mudstone with thin tabular interbeds of sandstone (Figs. 7A, 7B). The mudstone contains abundant marine microfossils including foraminifera and nannoplankton (Horng, 1991). We interpret the lower lithofacies as a product of

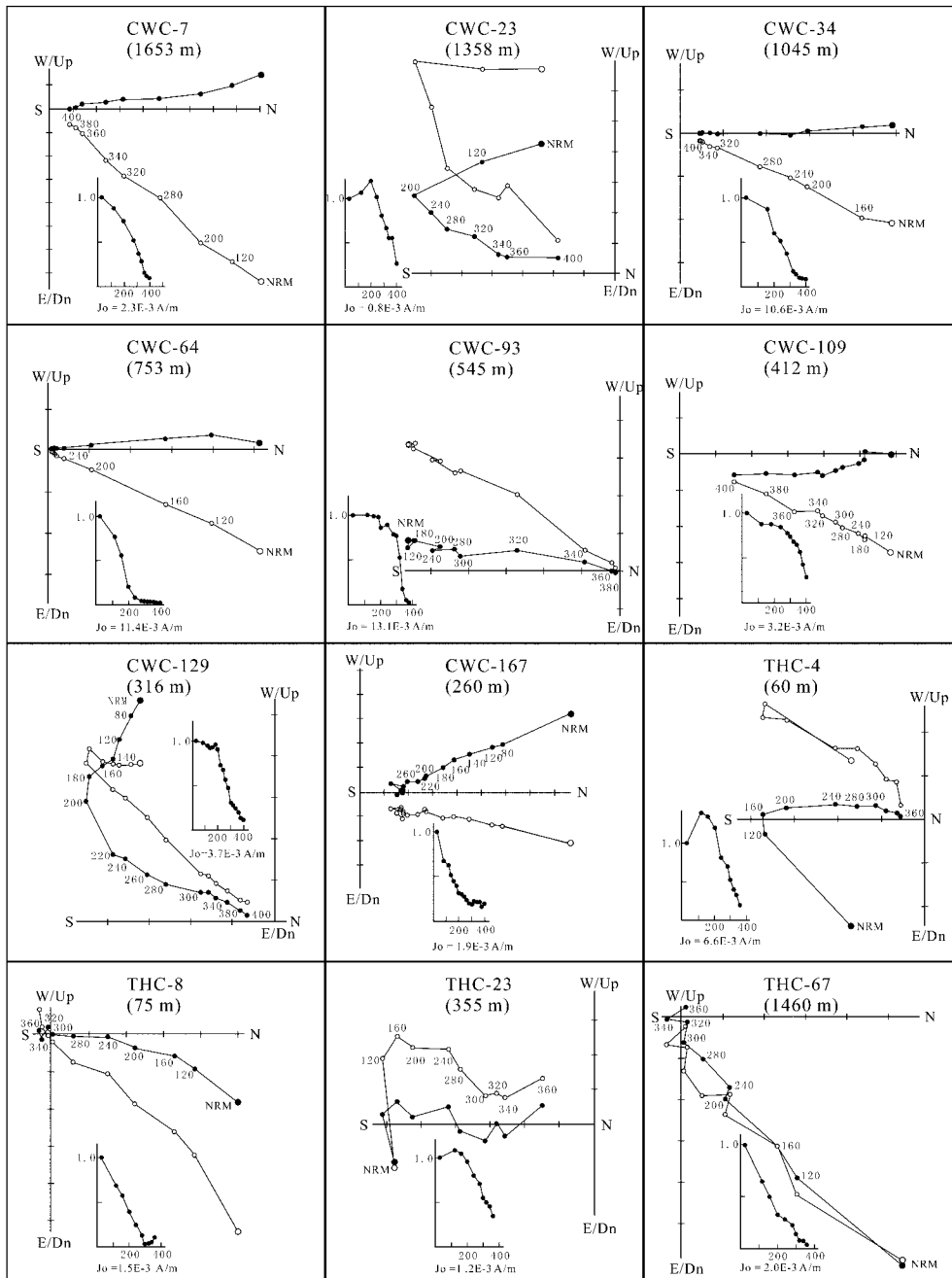


Figure 3. Representative thermal demagnetization diagrams of paleomagnetic samples from the Chengwenchi (CWC) and Tsaohuchi (THC) sections. Numbers in parentheses indicate stratigraphic position in meters. Demagnetization steps are shown with temperature ($^{\circ}$ C). Open and solid symbols represent projection of the vector end point on the vertical and horizontal planes, respectively. J_0 is intensity of NRM. Directions corrected for bedding tilt.

deposition in mud-rich lower offshore marine environments (e.g., Prave et al., 1996; Vera and Molina, 1998). The middle lithofacies is characterized by interbedded sandstone and mudstone. The sandstone beds increase in thickness and abundance up section, and they also become more channelized up section (Fig. 7C). The sandstones are bioturbated, but horizontal stratification and hummocky cross-stratification are preserved locally. Common trace fossils found in this lithofacies are *Paleophycus* sp. (ichnospecies), *Planolites* sp.,

Scolicia sp., and *Teichichnus* sp., and individual beds are characterized by low-diversity and low-abundance ichnofossils. We interpret these sandstones as storm deposits of middle offshore marine environments (e.g., DeRaaf et al., 1977; Bourgeois, 1980; Cheel and Leckie, 1993). The sandstone-rich storm beds grade upward into thick (1 to 2 m), tabular sandstones of the upper lithofacies (Fig. 7D). Sandstones of the upper lithofacies are highly bioturbated (Fig. 7E), have few sedimentary structures, and contain fossil hash. Common

trace fossils in this part of the package include *Paleophycus* sp., *Planolites* sp., *Subaucylindrichnus coronus*, *Teichichnus* sp., *Cylindrichnus concentricus*, and *Thalassinoides* sp., and individual beds are characterized by high-diversity and high-abundance ichnofossils. We interpret these sandstones as the product of deposition in upper offshore and near-shore marine environments (e.g., Leckie and Walker, 1982; Rossetti, 1997). In the uppermost part of our measured section, especially in the Erhchungchi and Liushuang Formations

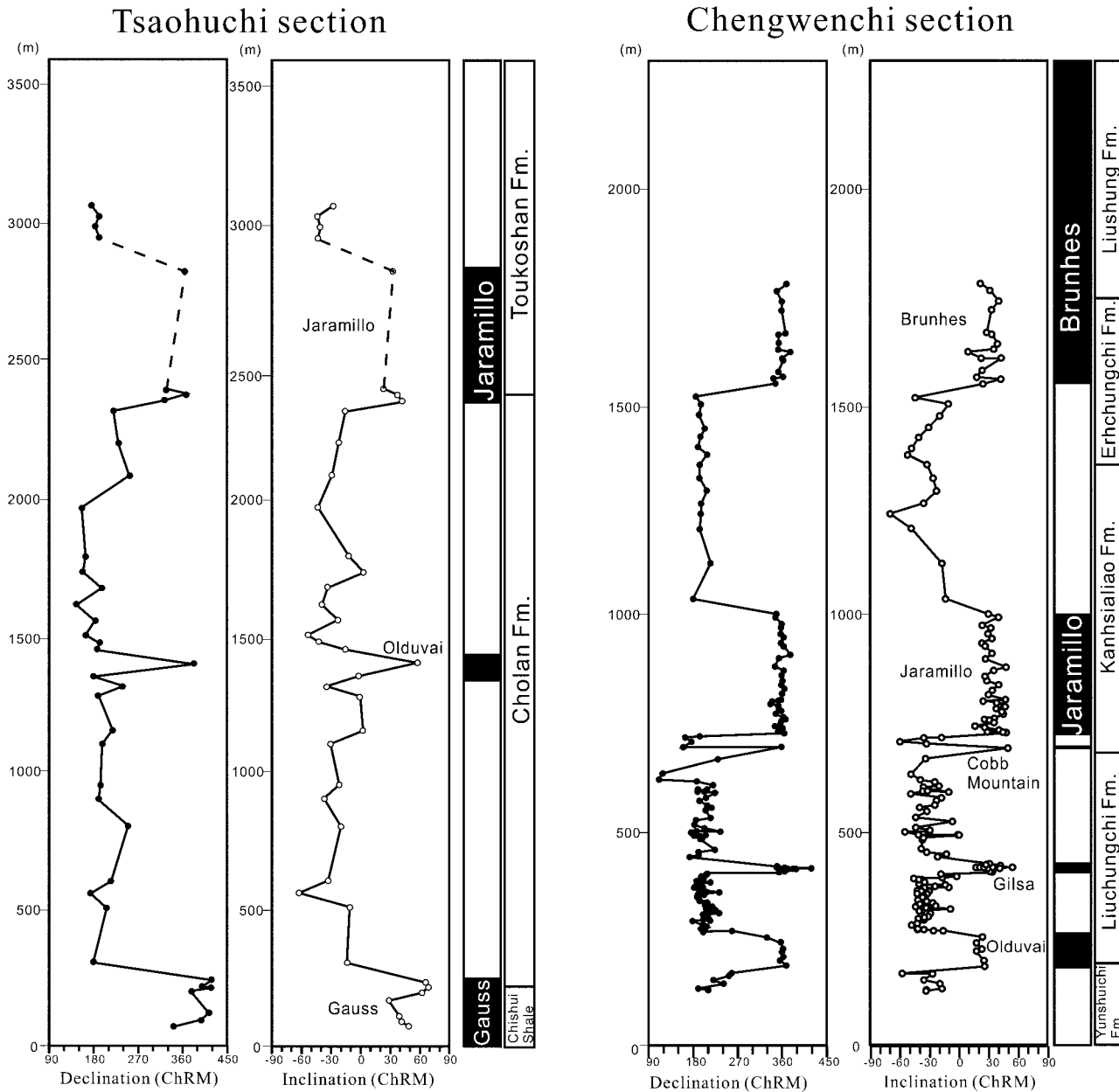
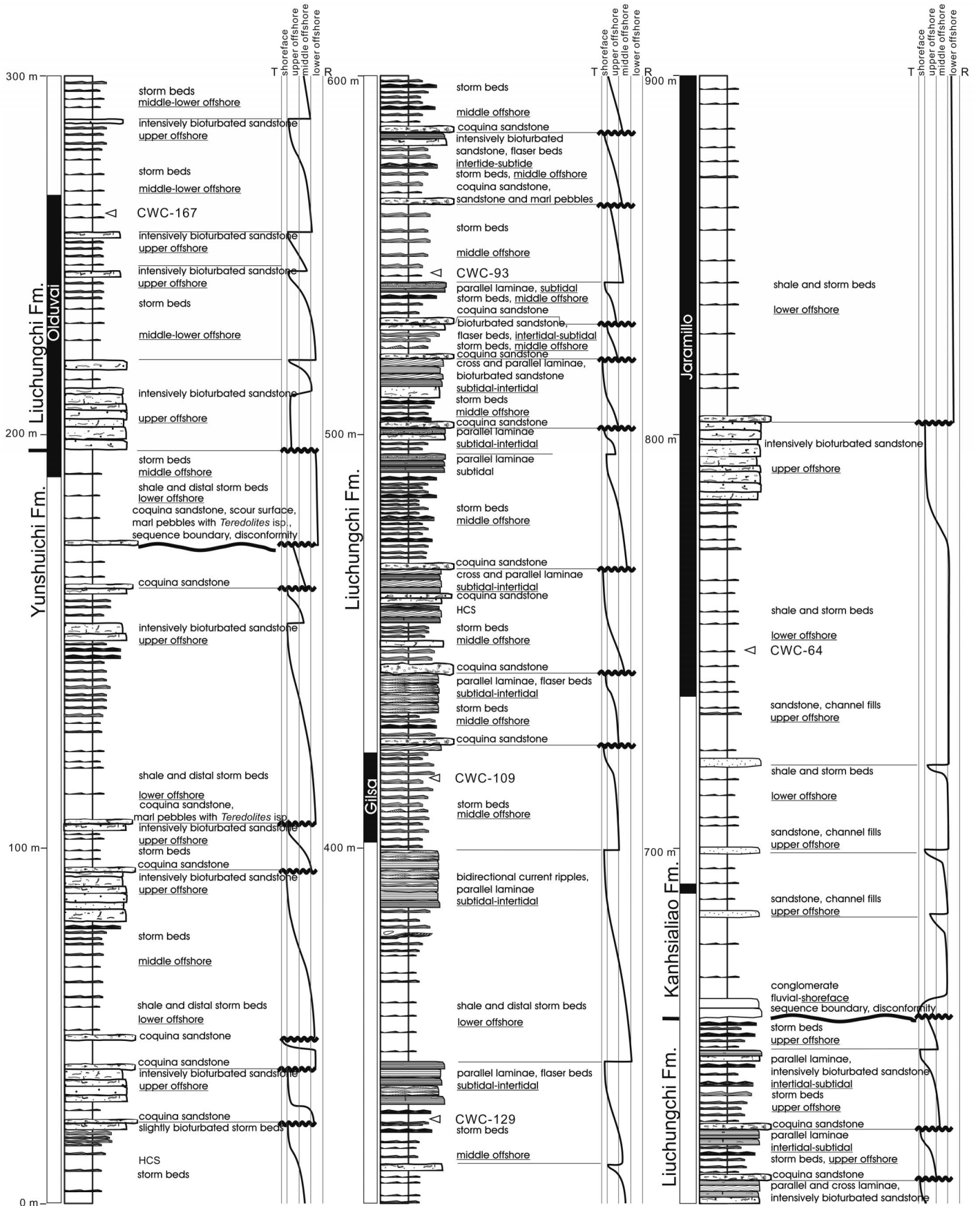


Figure 4. Stratigraphic plots of declination and inclination of the characteristic remanent magnetizations (ChRM) of the Tsaohuchi and Chengwenchi sections. Interpretation of magnetozones is based on the geomagnetic polarity time scale of Berggren et al. (1995) and microfossil datum events (Chen et al., 1977; Chi, 1978; Chang and Chi, 1983; Horng, 1991). Dashed line in the Tsaohuchi section represents conglomerate-dominated part of the section. Note that the Gilsa and Cobb Mountain chrons found in the Chengwenchi section were not located in the Tsaohuchi section. Better resolution in the Chengwenchi section is probably a function of sampling density. The finer grained deposits common in the Chengwenchi section are conducive to high-density sampling (184 sites) relative to the coarse-grained deposits that characterize the Tsaohuchi section (40 sites).

Figure 5. Log of measured Chengwenchi (Figs. 1B and 2) stratigraphic section from south-central Taiwan showing lithofacies, depositional environments, stratigraphic packages, stratigraphy, and paleomagnetic epochs. T—transgression, R—regression.



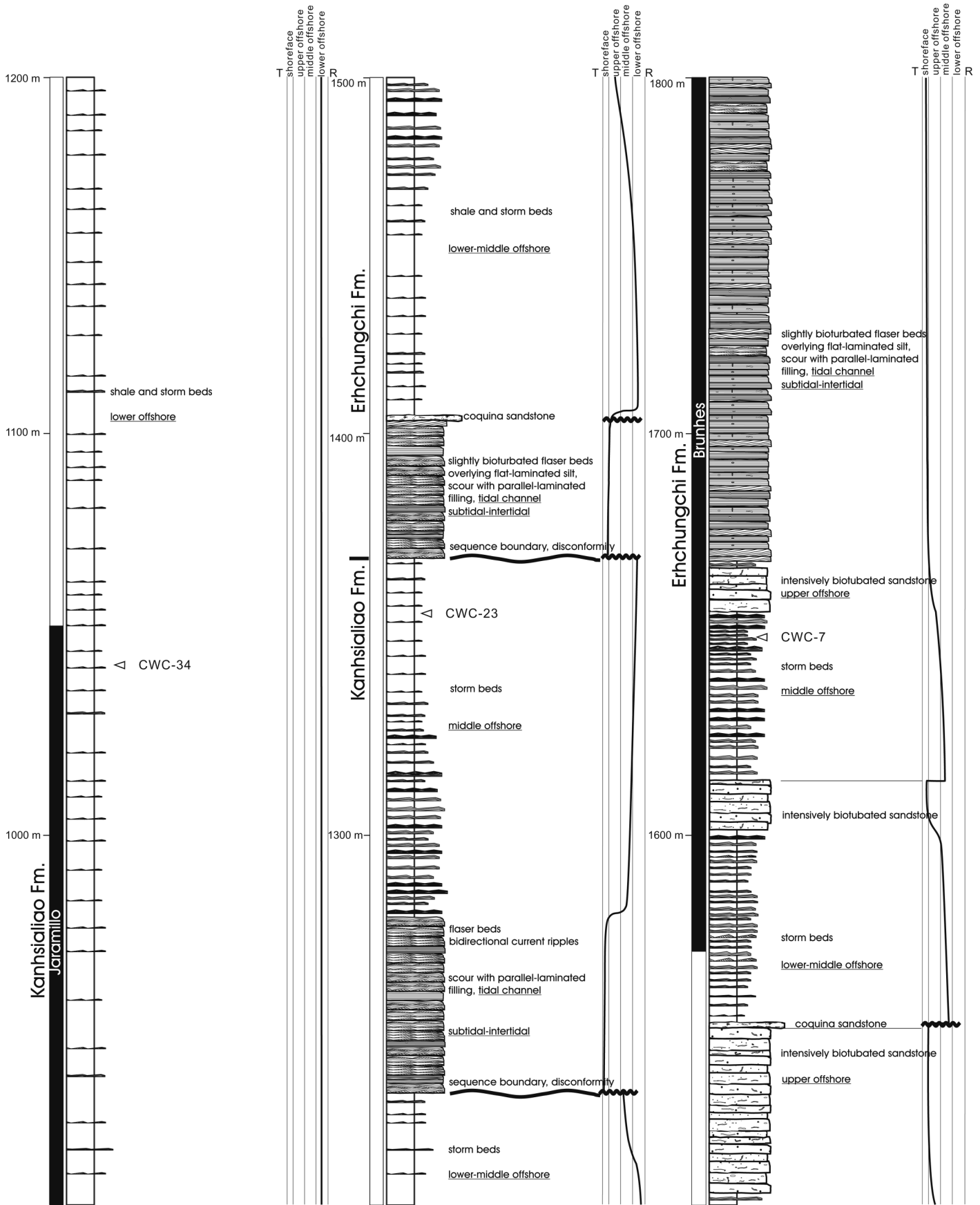


Figure 5. (Continued.)

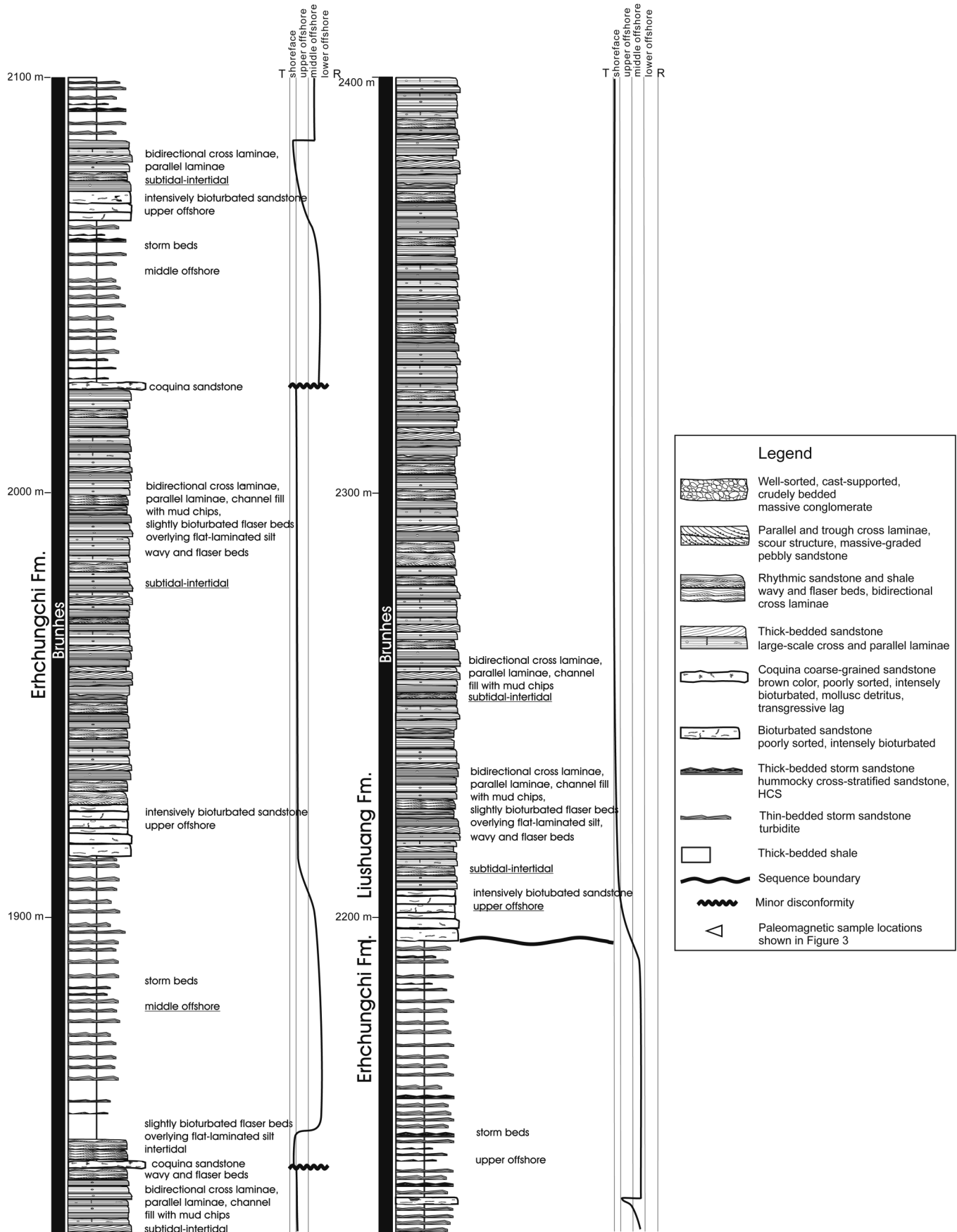


Figure 5. (Continued.)

(~1700 to 2400 m in Fig. 5), the upper lithofacies is overlain by wavy and flaser bedded, ripple-laminated sandstone and mudstone. This lithofacies is better developed in our measured section from north-central Taiwan (see next section).

The uppermost lithofacies of small-scale packages in south-central Taiwan is overlain by a thin horizon of coquina sandstone that marks the base of the overlying small-scale sequence. The coquina sandstones consist of extremely abundant articulated mollusk shells (Fig. 8A) and in situ scleractinian corals (Fig. 8B). The coquina sandstones are less than 50 cm thick, are extensively bioturbated, and were deposited directly on top of upper offshore or nearshore sandstone of the underlying small-scale sequence (Fig. 8 B and C). The coquina sandstones represent the basal unit of individual small-scale stratigraphic sequence and are overlain by offshore mudstone (Fig. 8C). We interpret the coquina sandstones as marine flooding intervals (e.g., Van Wagoner et al., 1988) associated with sea-level rise when sediment-starved upper offshore and nearshore sandstone surfaces were quickly colonized by mollusks and corals during transgression.

North-Central Taiwan: Proximal Foreland Basin Strata

Small-scale stratigraphic packages in north-central Taiwan consist of a lower lithofacies of interbedded mudstone and sandstone, a middle lithofacies of thickly bedded planar and trough cross-stratified sandstone, and an upper lithofacies consisting of ripple-laminated sandstone and mudstone (Fig. 6). These small-scale packages range in thickness from 20 to 150 m (Fig. 6). The lower lithofacies consists of tabular sandstone interbedded with mudstone that contains abundant foraminifera and nannoplankton microfossils. Individual sandstone beds are 50 cm to 1 m thick (Fig. 9A), are highly bioturbated (Fig. 9B), contain hummocky cross-stratification (Fig. 9C), and have well-defined scour surfaces (Fig. 9C). Common trace fossils in this lithofacies include *Planolites* isp., *Ophiomorpha* isp., *Paleophycus* isp., *Teichichnus* isp. and *Scolicia* isp. We interpret this lithofacies as lower and upper offshore marine storm beds (e.g., Leckie and Krystinick, 1989; Prave et al., 1996).

The storm beds grade upward into planar and trough cross-stratified sandstone (Fig. 9D)

and horizontally stratified sandstone (Fig. 9E) of the middle lithofacies. These sandstone beds are tabular at outcrop scale and may be up to 10 m thick (Fig. 9F). Trace fossils common to the middle lithofacies include *Ophiomorpha* isp. and *Skolithos* isp. These strata are interpreted as nearshore marine sandstones that formed above storm wave base (e.g., Clifton, 1981; McCubbin, 1982; Johnson and Levell, 1995). The nearshore sandstone component of individual small-scale stratigraphic packages increases up-section (Fig. 6).

Overlying the nearshore sandstone lithofacies are laminated sandstone and mudstone (Fig. 6). This lithofacies contains flaser and wavy bedding (Fig. 9G), mud-draped ripple foresets (Fig. 9H), and thin (<50 cm), broadly lenticular sandstone channels (Fig. 9I). We interpret this lithofacies as the product of deposition in tidal-flat and estuarine environments (e.g., Clifton, 1982; Dalrymple, 1992). In the uppermost part of our measured section (Toukoshan Formation of Fig. 6), the estuarine deposits are overlain by clast-supported, well-organized conglomerates (Fig. 9J), which become more abundant up section (Fig. 6). Finer-grained interbeds within the conglomerate contain nonmarine megafloora and fossilized teeth, bones, and horns of elephant, deer, and rhinoceros. We interpret these channelized conglomerates as braided stream and stream-dominated alluvial fan deposits (e.g., Miall, 1977; Ridgway and DeCelles, 1993).

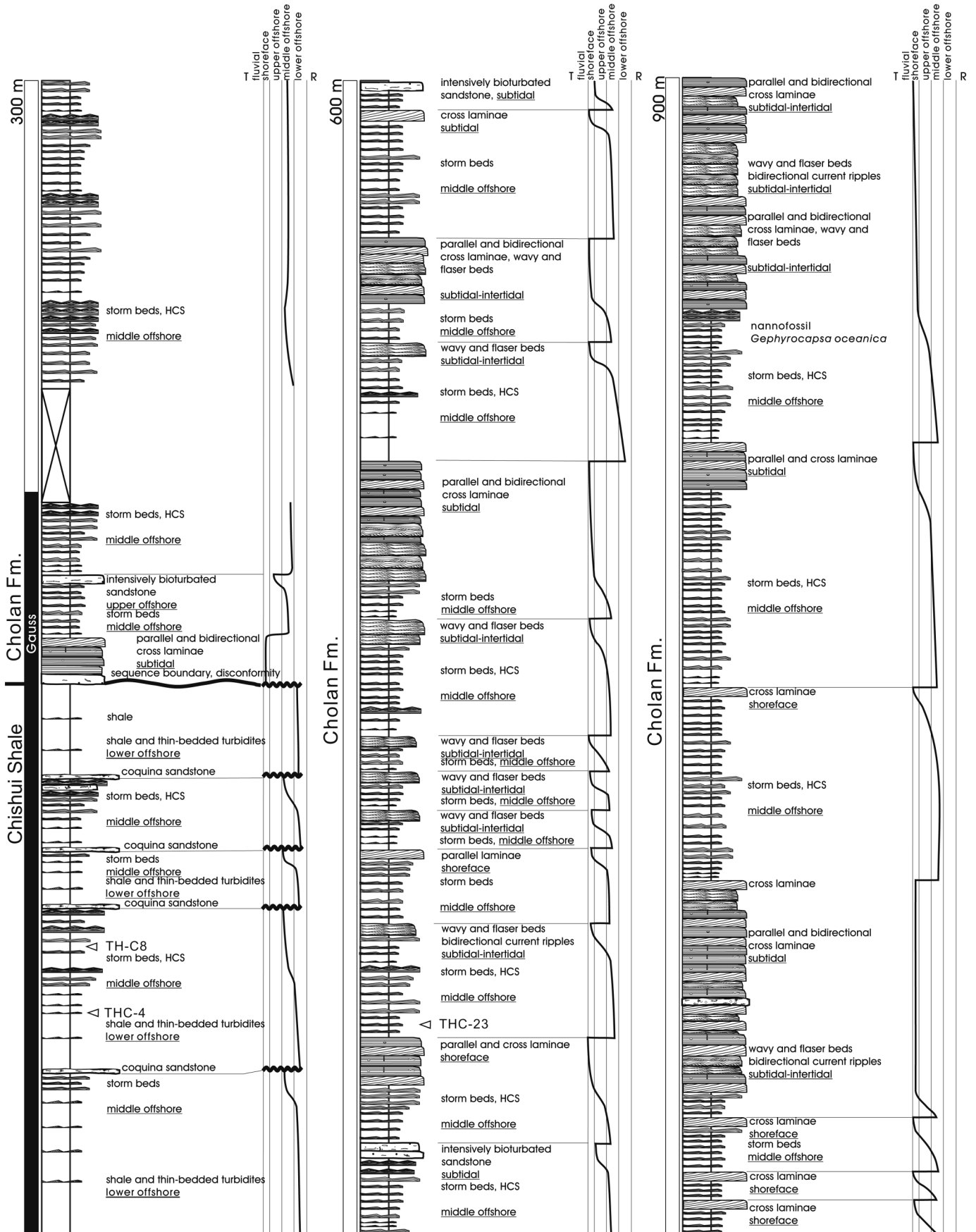
Intermediate-Scale Stratigraphic Packages

Intermediate-scale stratigraphic packages are defined by unconformity-bounded units of strata that range in thickness from 150 to 1000 m. These packages are extremely well exposed in our representative measured section from south-central Taiwan (Fig. 5) and can be identified in a nearby northwest-southeast seismic line through the Pliocene-Pleistocene foreland basin deposits (Fig. 10). The stratigraphic interpretation and location of each unconformity on the seismic section was determined by unpublished biostratigraphic data and geophysical well logs from two wells, drilled by the Chinese Petroleum Corporation, located near the line of the seismic profile (Fig. 1B). To determine if unconformities identified on the seismic profile could be documented in outcrop, we studied

correlative stratigraphic positions in nearby outcrops based on previous published biostratigraphy (Chen et al., 1977; Chi, 1978; Chang and Chi, 1983; Horng, 1991). Unconformities identified in the subsurface of the foreland basin are present in outcrop and define erosional surfaces with several hundred meters of relief. These erosional surfaces define several major Pliocene-Pleistocene incised-valley systems in the foreland basin of south-central Taiwan (Fig. 10). We have been able to trace all of the high-relief unconformities for ~40 km along strike in outcrop exposures in the general area of our measured section. Five episodes of major incision in the foreland basin, recognized on the seismic profile and in outcrop, are represented by unconformities located near the top of the Yunshuichi Formation, the top of the Liuchungchi Formation, the upper-middle and top of the Kanhsialiao Formation, and the top of the Erhchungchi Formation (Figs. 5, 10). Note in Figure 10 that these high-relief unconformities commonly truncate underlying well-developed reflectors. Truncation is well illustrated, for example, at the unconformity at the top of the Liuchungchi Formation (yellow line in Fig. 10) and at the unconformity in the upper-middle part of the Kanhsialiao Formation (black line in Fig. 10).

The lowest major erosional surface in our measured section along the Chengwenchi River is near the top of the Yunshuichi Formation (at 170 m in Fig. 5) and is stratigraphically equivalent to the red line in Figure 10. At this locality, the unconformity near the top of the Yunshuichi Formation is characterized by a zone of disarticulated mollusk shells (Fig. 11A), marl clasts that are encrusted with barnacles and have boreholes of *Teredolites* isp. (Fig. 11A), and by extensive bioturbation. The next major erosional unconformity in this section is at the top of the Liuchungchi Formation (at 640 m in Fig. 5) and is stratigraphically equivalent to the yellow line in Figure 10. This contact is an angular unconformity (Fig. 11, B and C) at the Chengwenchi measured-section locality. The underlying Liuchungchi Formation dips 88° southwest, whereas the overlying Kanhsialiao Formation dips 57° southwest. The contact between the two formations is a deeply incised channel that is filled with sandstone of the Kanhsialiao For-

Figure 6. Log of measured Tsaohuchi (Figs. 1B and 2) stratigraphic section from north-central Taiwan showing lithofacies, depositional environments, stratigraphic packages, stratigraphy, and paleomagnetic epochs. T—transgression, R—regression, HCS—hummocky cross-stratification.



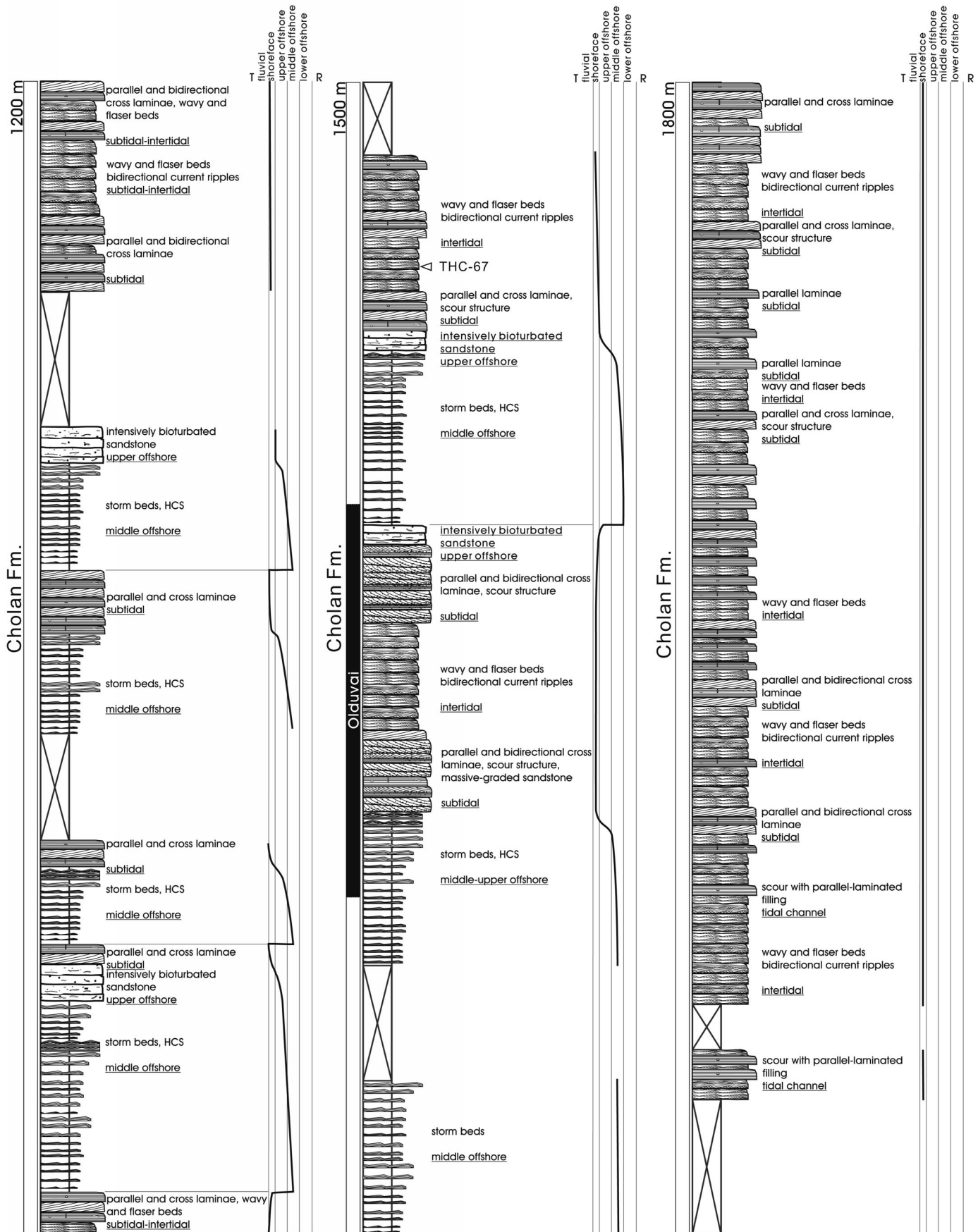


Figure 6. (Continued.)

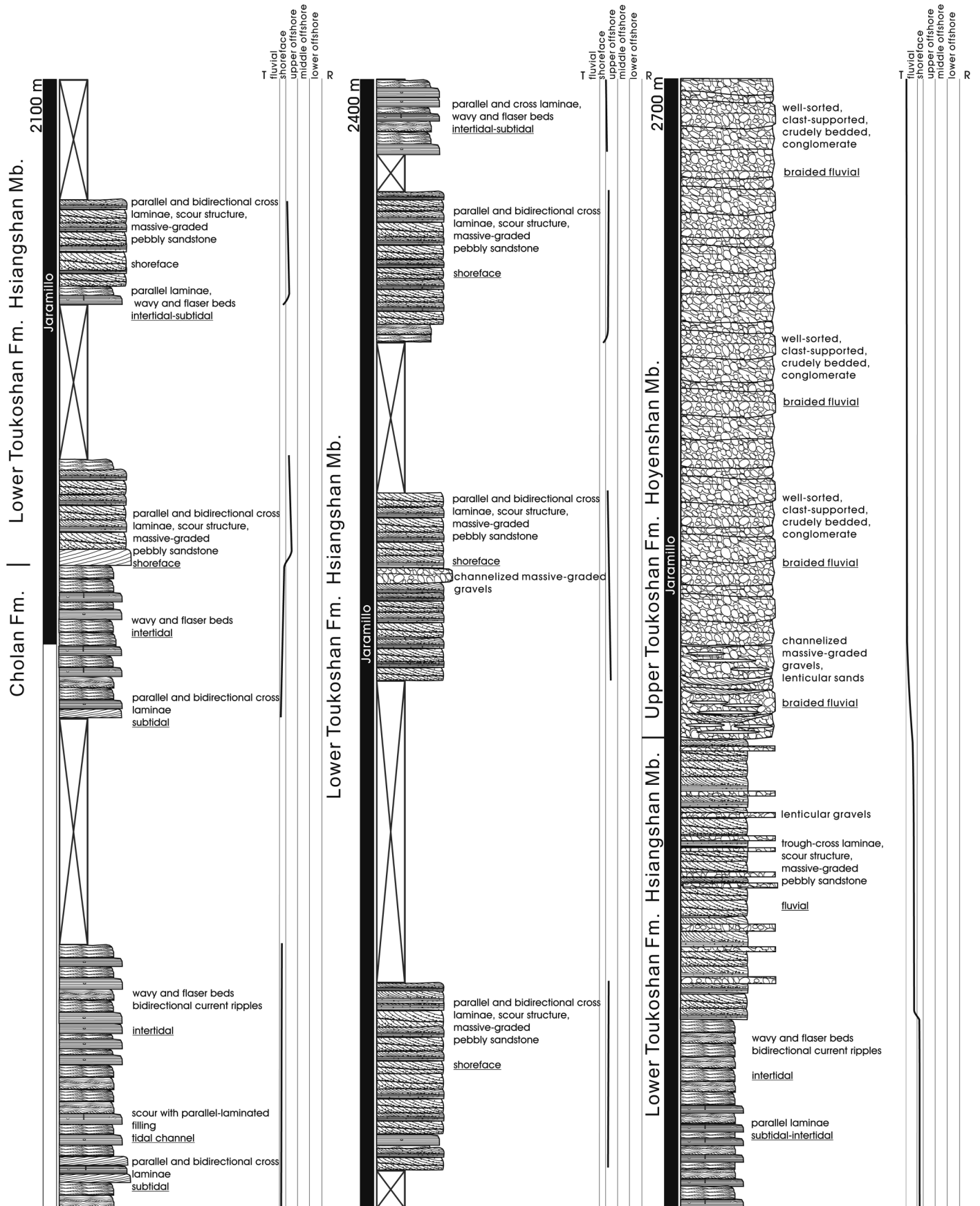


Figure 6. (Continued.)

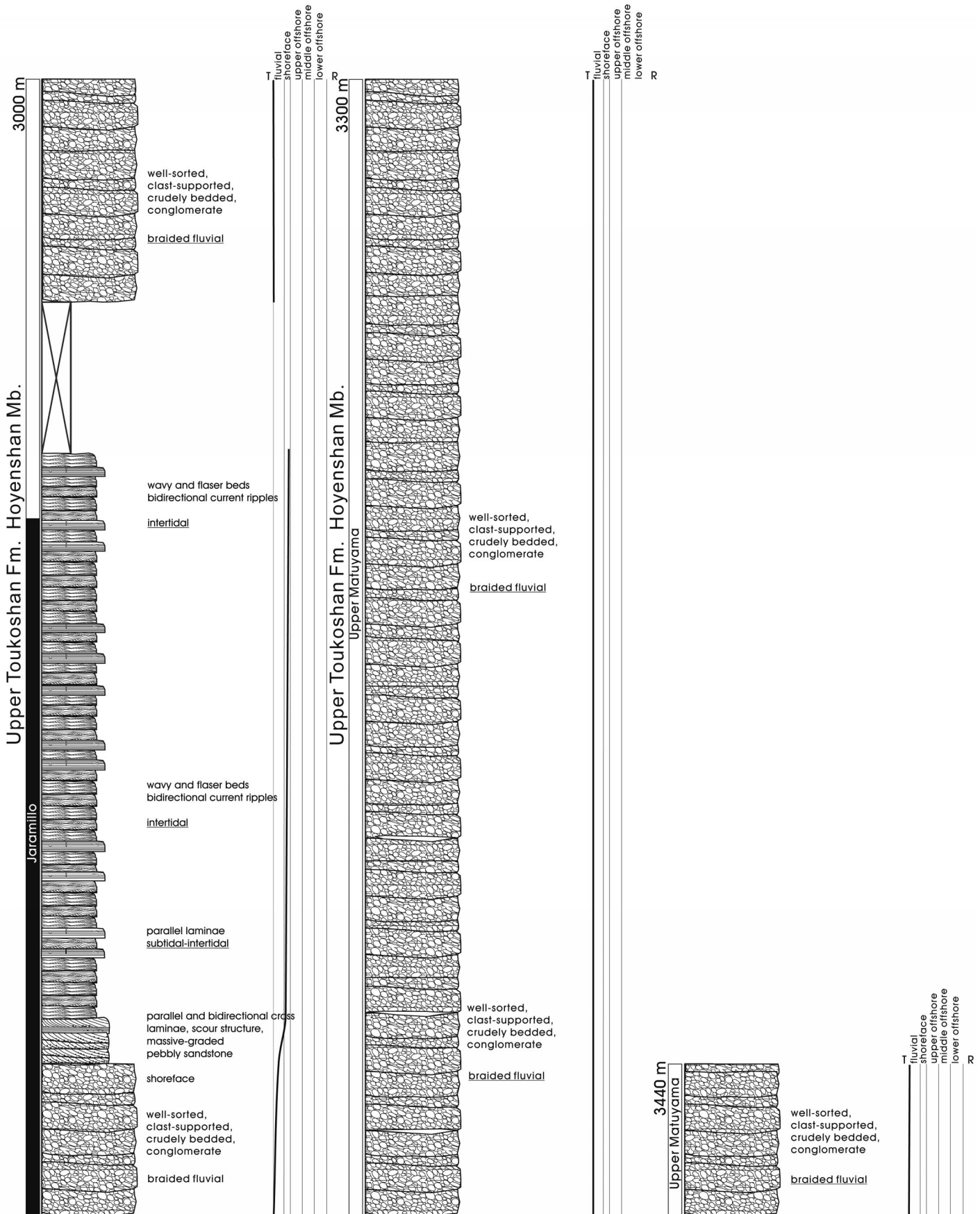


Figure 6. (Continued.)

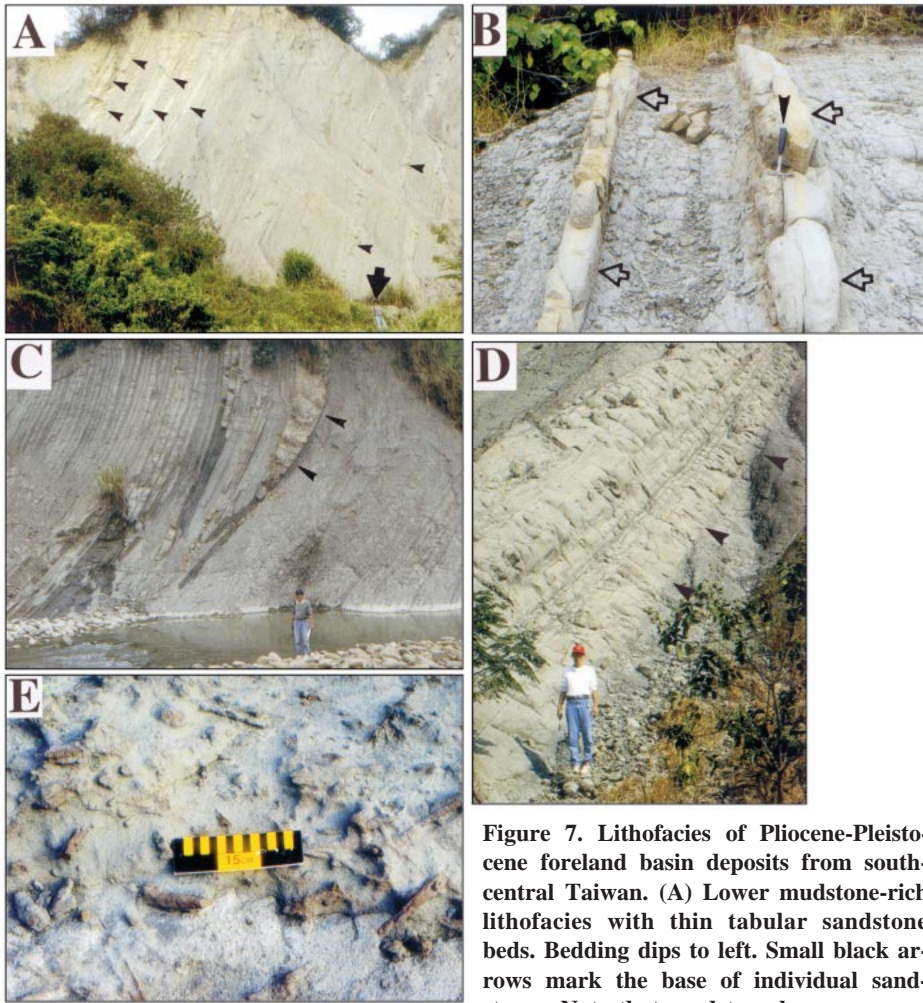


Figure 7. Lithofacies of Pliocene-Pleistocene foreland basin deposits from south-central Taiwan. (A) Lower mudstone-rich lithofacies with thin tabular sandstone beds. Bedding dips to left. Small black arrows mark the base of individual sandstones. Note that sandstone becomes more common up section. Large black arrow points to a person, for scale. (B) Close-up of sandstone storm beds (resistant units) interbedded with marine mudstone (recessive gray units). Open arrows point toward base of sandstones. Hammer (solid arrow) is 28 cm long. (C) Transition from lower mudstone lithofacies to middle interbedded sandstone and mudstone lithofacies. Arrows point toward the contact between the two lithofacies. Note the channelized geometry of storm bed at the contact. (D) Thick-bedded sandstone-dominated upper lithofacies. Bedding dips to left. Sandstone is tabular and contains marine fossil hash. Arrows indicate base of tabular sandstone. (E) Highly bioturbated sandstone of upper lithofacies. Trace fossils are *Paleophycus* isp. and *Thalassinoides* isp.

mation (Fig. 11C). Along strike, ~35 km to the north of our measured section, the contact between the Liuchungchi and Kanhsialiao Formations is also well exposed. At this location, the contact is conformable and the overlying Kanhsialiao Formation consists of a cobble conglomerate. The next major unconformity that is well exposed at the Chengwenchi measured-section locality is in the Kanhsialiao Formation (at 1225 m in Fig. 5) and is stratigraphically equivalent to the black line in Figure 10. In the area of our measured section, this surface is a high-relief disconformity (Fig. 12A) with an

abrupt change in lithofacies across the disconformity. The Kanhsialiao Formation immediately beneath the contact consists of mudstone-rich lower offshore marine lithofacies with abundant marine microfossils (Fig. 12A). Lithofacies directly above the unconformity are ripple-laminated sandstones (Fig. 12A) that contain abundant climbing ripples (Fig. 12B) and bimodal flow indicators (Fig. 12C) indicative of estuarine and tidal-flat deposition. Similar abrupt lithofacies changes from lower offshore marine to nearshore estuarine and shoreface deposits are found across several

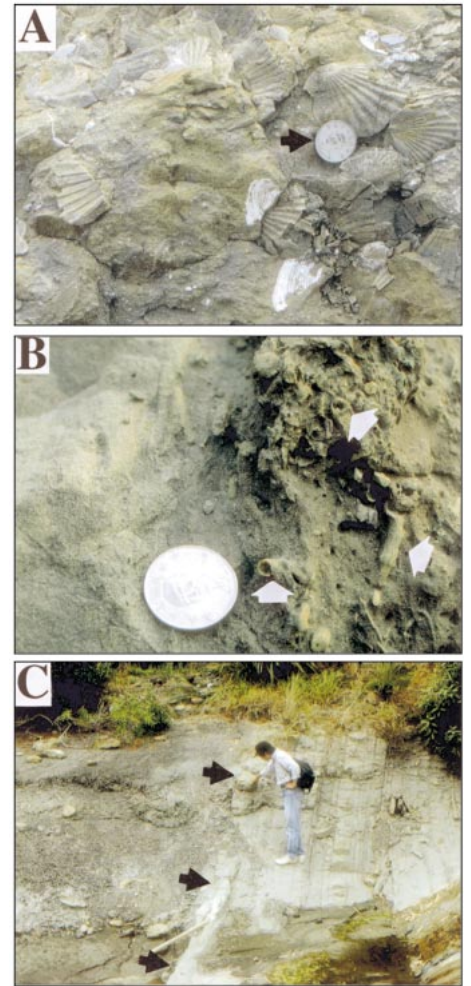


Figure 8. Lithofacies of Pliocene-Pleistocene foreland basin deposits from south-central Taiwan. (A) Bedding surface view of coquina sandstone with abundant mollusk shells. Coin (arrow) is 20 mm in diameter. (B) Cross-sectional view of coquina sandstone. Bedding dips steeply to the right. The coquina sandstone horizon begins to the right of the coin (20 mm diameter). Note the abundance of scleractinian corals. Arrows point to larger intact corals. Left of the coin is the top of the sandstone-dominated upper lithofacies of the underlying small-scale stratigraphic package. (C) Contact between two small-scale stratigraphic packages. Bedding dips steeply; stratigraphic up is to the left. The person is standing on the sandstone-dominated upper lithofacies of the underlying small-scale stratigraphic package. Arrows point to the location of coquina sandstone that marks the base of the overlying package. Overlying the coquina sandstone are gray marine mudstones representing the mudstone-rich lower lithofacies of the overlying small-scale stratigraphic package.

of the other major unconformities within the foreland basin deposits (~640, ~1365, and ~2190 m in Fig. 5). Approximately 20 km along strike at Cow Mountain, the major unconformity at ~1225 m in Figure 5 is well exposed; lower offshore marine mudstone is unconformably overlain by tidal sandstone that contains large rip-up clasts of the underlying mudstone (Fig. 12D).

Large-Scale Stratigraphic Packages

Large-scale stratigraphic packages are present in our measured sections in both the north-central and south-central parts of the Taiwan foreland basin. These packages consist of overall upward-coarsening and upward-shallowing trends (Figs. 2, 5, 6). In south-central Taiwan, the lower and middle parts of the section (the Yunshuichi, Liuchungchi, and

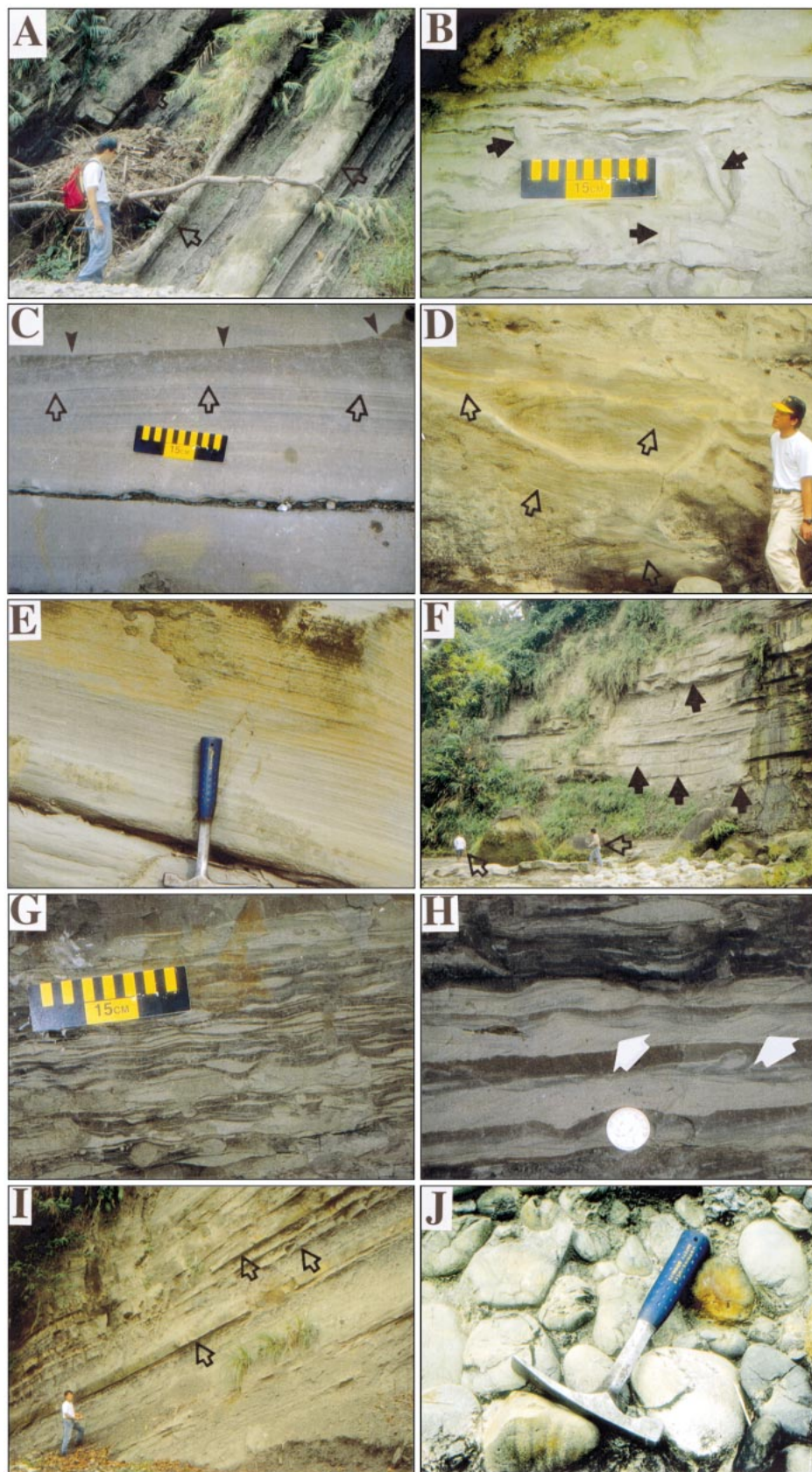


Figure 9. Lithofacies of Pliocene-Pleistocene foreland basin deposits from north-central Taiwan. (A) Lower lithofacies of tabular sandstone interbedded with mudstone. Arrows point toward bases of individual sandstone beds. (B) Extensive bioturbation common in proximal storm beds. Arrows point toward well-developed burrows of *Thalassinoides* isp. (C) Hummocky cross-stratification of proximal storm beds. Open arrows point toward a convex-upward stratification surface. Solid arrows point toward a well-defined scour surface typical of the proximal storm beds. (D) Trough cross-stratified sandstone of middle lithofacies interpreted as nearshore sandstone. Arrows point toward well-defined limbs of trough cross-stratification. (E) Horizontal stratification of nearshore sandstone. The hammer is 28 cm long. (F) Thick-bedded, tabular sandstones of the middle lithofacies. Solid arrows point toward the base of individual sandstones. Open black arrows point to people for scale. (G) Wavy and flaser bedding characteristic of the upper lithofacies that we interpret as having been deposited in tidal-flat and estuarine environments. (H) Ripple stratification common in upper lithofacies. Arrows point toward mud-draped ripple foresets. The coin is 20 mm in diameter. (I) Thin, broad, lenticular channels interbedded with ripple-laminated sandstone and mudstone of upper lithofacies. Arrows point toward base of individual sandstone beds. Bedding dips to left. Person in lower left for scale. (J) Clast-supported, well-organized fluvial conglomerate common in the upper part of our measured section from north-central Taiwan.

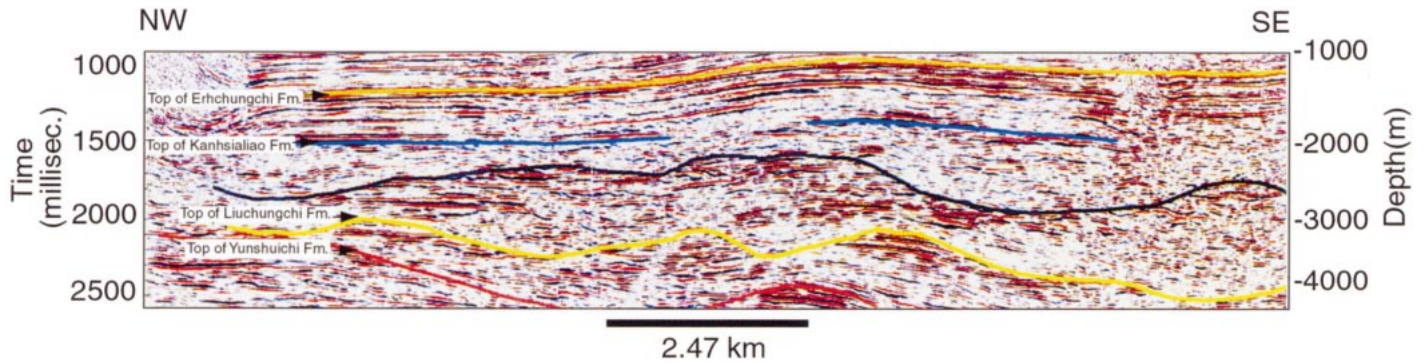


Figure 10. Interpreted northwest-southeast-oriented seismic profile (SW-1 in Fig. 1B) of Pliocene-Pleistocene foreland basin deposits in south-central Taiwan. This profile shows almost the entire Pliocene-Pleistocene foreland basin section. The stratigraphically oldest deposits of the foreland basin are the Yunshuichi Formation. The stratigraphically youngest deposits, the top of the Liushung Formation, are stratigraphically above the view of the seismic profile. Each colored line represents an unconformity that we have interpreted in the section. Each of the interpreted subsurface unconformities has a stratigraphically equivalent unconformity exposed in nearby outcrops. Interpretation of stratigraphic formations shown on the seismic section is consistent with biostratigraphic data and geophysical well logs from two nearby petroleum wells (Fig. 1B). Note that the horizontal and vertical scales are approximately equal; the section has little vertical exaggeration. The migrated seismic profile was acquired and processed by the Chinese Petroleum Corporation.

Kanhsialiao Formations in Fig. 5) are dominated by offshore marine mudstone and subordinate interbedded distal sandstone storm deposits. In the upper part of the section (the Erchungchi and Liushuang Formations in

Fig. 5), upper offshore marine sandstone and tidal sandstone increase in thickness and abundance relative to mudstone-rich, deeper offshore marine lithofacies. A similar trend can be seen in our measured section from north-

central Taiwan (Fig. 6) but with a different lithofacies distribution. There, the lower part of the section is dominated by proximal offshore sandstone storm beds and estuarine lithofacies, whereas in the upper part of the section nearshore marine sandstone and fluvial conglomerate dominate (Fig. 6).

DISCUSSION

Our analysis of Pliocene-Pleistocene strata documents several scales of stratigraphic packages and unconformities that we interpret as the products of relative changes of sea level in the Taiwan foreland basin. Relative changes of sea level may be a function of eustasy, tectonics, and/or sediment supply (Plint et al., 1992).

Interpretation of Small-Scale Stratigraphic Packages

We recognize two variations of small-scale stratigraphic packages in different parts of the Taiwan foreland basin. Small-scale packages in the more distal foreland basin deposits (south-central Taiwan) consist of a basal coquina sandstone and lower offshore marine mudstone-rich lithofacies, a middle lithofacies of interbedded sandstone storm beds and mudstone interpreted as middle offshore marine deposits, and an upper sandstone-dominated lithofacies characteristic of upper offshore and nearshore marine environments (Fig. 13). The top of the upper lithofacies is overlain by a coquina sandstone that marks the beginning of the next small-scale package (Fig. 13). In the more proximal deposits of the foreland basin

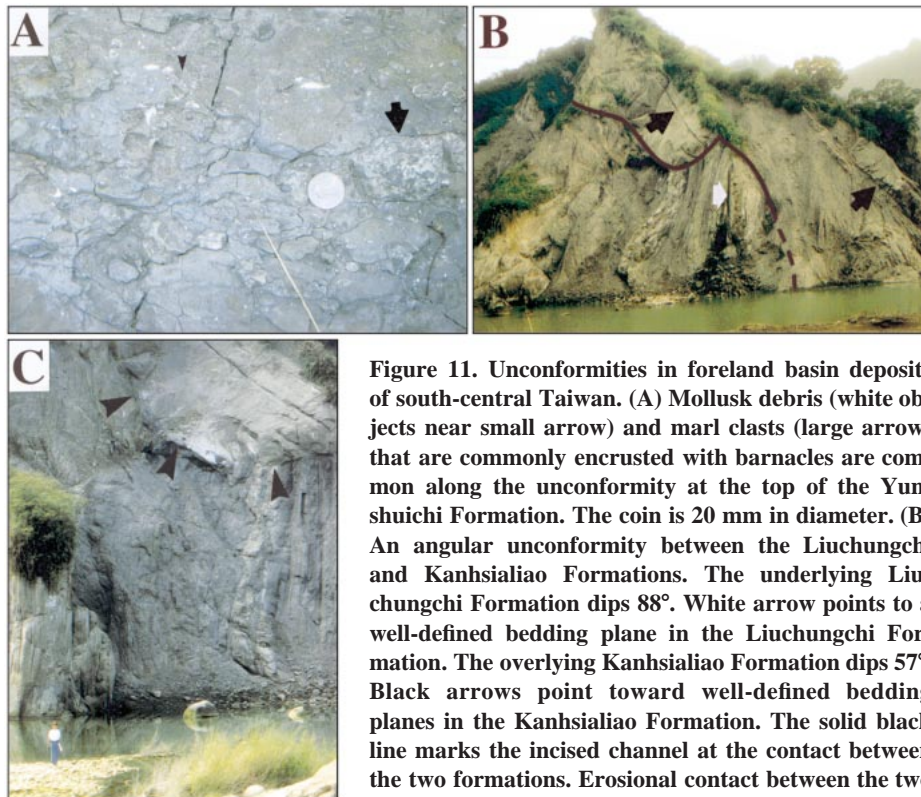


Figure 11. Unconformities in foreland basin deposits of south-central Taiwan. (A) Mollusk debris (white objects near small arrow) and marl clasts (large arrow) that are commonly encrusted with barnacles are common along the unconformity at the top of the Yunshuichi Formation. The coin is 20 mm in diameter. (B) An angular unconformity between the Liuchungchi and Kanhsialiao Formations. The underlying Liuchungchi Formation dips 88°. White arrow points to a well-defined bedding plane in the Liuchungchi Formation. The overlying Kanhsialiao Formation dips 57°. Black arrows point toward well-defined bedding planes in the Kanhsialiao Formation. The solid black line marks the incised channel at the contact between the two formations. Erosional contact between the two formations is covered by float in the lower part of the outcrop (dashed line). Person in C indicates scale. (C) Close-up of center of outcrop in B showing angular unconformity. Black arrows outline the incised channel.

outcrop (dashed line). Person in C indicates scale. (C) Close-up of center of outcrop in B showing angular unconformity. Black arrows outline the incised channel.

(north-central Taiwan), a similar vertical change in lithofacies is observed, but with slightly different lithofacies types (Fig. 13). In this part of the foreland basin, small-scale stratigraphic packages consist of a lower lithofacies of interbedded sandstone storm beds and mudstone interpreted as lower to middle offshore marine deposits, a middle lithofacies of thickly bedded hummocky, planar, and trough cross-stratified sandstone representative of upper offshore and nearshore marine depositional environments, and an upper lithofacies characterized by tidal ripple-laminated sandstone and mudstone (Fig. 13). The thin coquina sandstones common in more distal offshore marine deposits of the foreland basin are not as well developed in the more proximal nearshore marine and nonmarine deposits.

Both variations of small-scale stratigraphic packages that we have documented contain an upward-shallowing succession of lithofacies. We interpret these packages as parasequences of the sequence stratigraphy nomenclature. A parasequence is a relatively conformable succession of genetically related beds or bed sets bounded by marine-flooding surfaces and their correlative surfaces (Van Wagoner et al., 1988). A marine-flooding surface is a surface that separates younger from older strata; across it there is evidence of an abrupt increase in water depth (Van Wagoner et al., 1988). The coquina sandstones of south-central Taiwan represent marine-flooding surfaces in our interpretation of the foreland basin deposits. We interpret the upward-shallowing, small-scale stratigraphic packages documented in the Taiwan Pliocene-Pleistocene foreland basin as representing the transition from transgressive system tract deposits (Fig. 13) associated with a rapid rise in relative sea level to highstand systems tract deposits associated with the late part of relative sea-level rise, stillstand, and the early part of a fall (sensu Van Wagoner et al., 1988). The shoreface and upper offshore deposits documented in small-scale stratigraphic packages of the distal foreland basin (Fig. 13) are interpreted as forced regressive systems tract deposits and represent shelf sedimentation during sea-level fall (sensu Hunt and Tucker, 1992; Posamentier et al., 1992; Naish and Kamp, 1997). Similar small-scale packages defined by changes from deeper-marine to shallow marine or nonmarine lithofacies have been described in deposits of several other foreland basins (e.g., Leckie, 1986; Swift et al., 1987; Plint, 1988; Gardner et al., 1992). The apparent poorer development of marine flooding surfaces in the more proximal foreland basin deposits may be a function of our inability to recognize these surfaces where they are not clearly marked by an abrupt

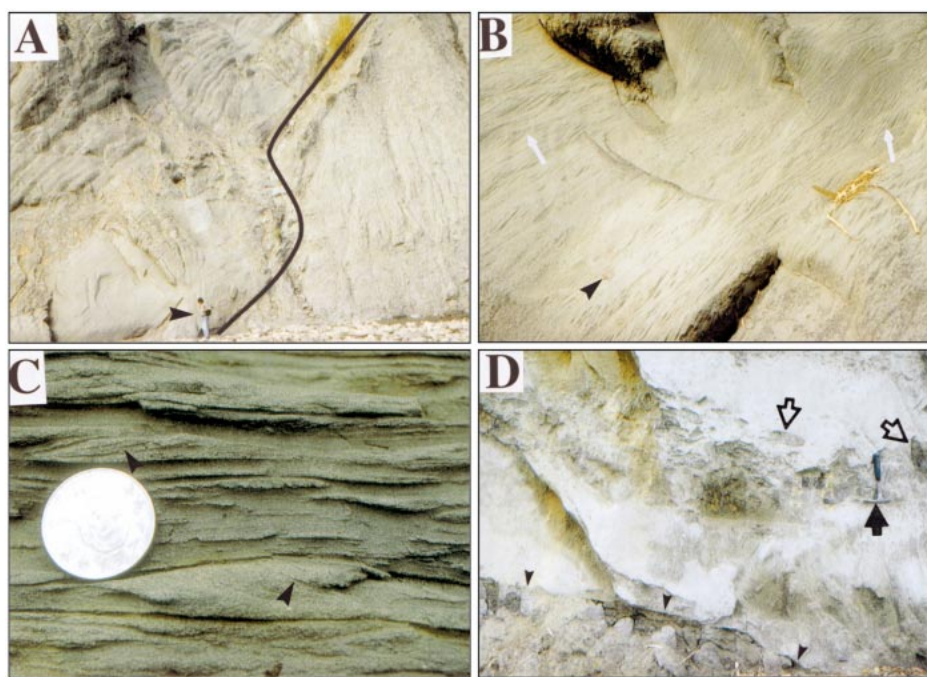


Figure 12. Unconformities and associated lithofacies in foreland basin deposits of south-central Taiwan. (A) High-relief unconformity in the Kanhsialiao Formation. Bedding dips to the left. Black line outlines the contact between underlying gray marine mudstones and overlying tidal ripple-laminated sandstones. (B) Close-up of ripple-laminated sandstones above the unconformity shown in A. White arrows point toward areas where climbing ripples are well exposed. Black arrow points toward coin (20 mm diameter). (C) Close-up of ripple-laminated sandstones with bimodal flow indicators. Note that ripple foresets above the 20 mm-diameter coin (arrow) dip to the left, whereas ripple foresets below the coin (arrow) dip to the right. (D) Same unconformity as shown in A but 20 km away. Note the sharp erosional contact (small black arrows) between the marine mudstones and overlying tidal sandstones. Open black arrows point toward large rip-up clasts of marine mudstone that are common in the tidal sandstone above the unconformity. The hammer is 28 cm long.

change in grain size and localization of fossils along a discrete horizon, as found in the offshore marine deposits.

Small-scale stratigraphic packages are best developed in the lower part of the Pliocene-Pleistocene foreland basin deposits represented by the Yunshuichi and Liuchungchi Formations (Fig. 5). Roughly, 19 to 20 small-scale packages were deposited and preserved during deposition of the Liuchungchi Formation (~195 to ~640 m in Fig. 5). The base of the Liuchungchi Formation is located just above the base of the Olduvai polarity epoch (~190 m in Fig. 5), according to our magnetostratigraphic data. The base of the Olduvai polarity epoch is at ~1.95 Ma (Shackleton et al., 1995a). The top of the Liuchungchi Formation coincides with the base of the nanoplanktonic biozone for the small *Gephyrocapsa* spp., which is at ca. 1.22 Ma (Hornig, 1991). Our data, therefore, indicate that ~19 to 20 packages were deposited over 730 k.y., so the average duration of small-scale stratigraphic

packages in the lower part of the Taiwan foreland basin deposits was on the order of 38.4 to 36.5 k.y. At a more detailed scale, roughly four complete small-scale packages were deposited from the top of the Olduvai polarity epoch (slightly older than 1.77 Ma; at 260 m in Fig. 5) to the Gilsa polarity epoch (~1.62 Ma; at 400 m in Fig. 5). Time-averaged small-scale packages during this time range had durations on the order of ~37.5 k.y. We interpret most of the small-scale stratigraphic packages of the Taiwan Pliocene-Pleistocene foreland basin to be a product of eustatic sea-level variation on the basis of their average time duration. Glacial-eustatic sea-level changes, related to growth and decay of ice sheets, are on the order of 10 to 100 k.y., whereas sea-level changes related to tectonics are often on the order of 100 k.y.–100 m.y. (Hayes et al., 1976; Revelle, 1990). Small-scale packages documented in our study may be similar to stratigraphic packages in the Pliocene-Pleistocene Wanganui basin of New Zealand,

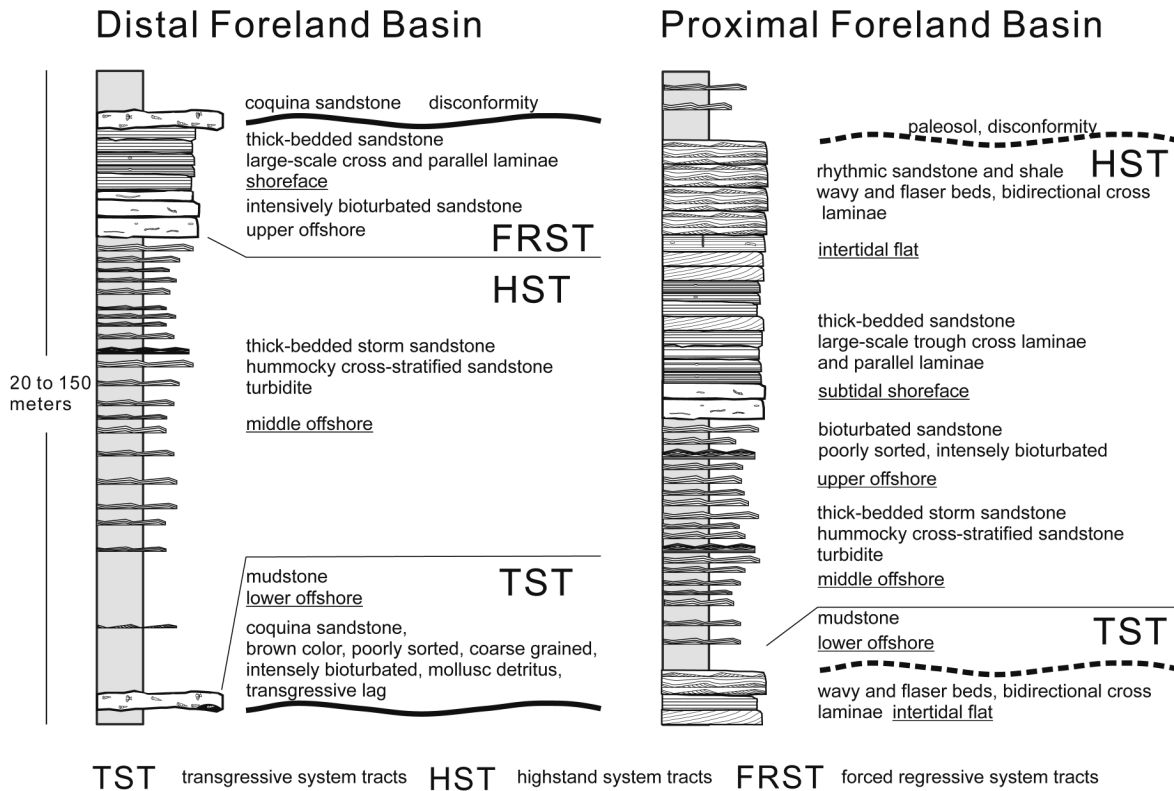


Figure 13. Comparison of small-scale stratigraphic packages from distal and proximal deposits of the Pliocene-Pleistocene foreland basin of Taiwan. Bases of distal small-scale packages consist of a fossil-rich coquina sandstone and lower offshore mudstones that we interpret as part of the transgressive systems tract (TST). Interbedded sandstone storm beds and middle offshore mudstones define the highstand system tract (HST) in the distal foreland basin. The HST is overlain by a sandstone-dominated lithofacies characteristic of upper offshore and nearshore marine environments that we interpret as part of the forced regressive system tract. In the more proximal part of the foreland basin, a lower lithofacies consisting of thin sandstone storm beds and lower offshore mudstones defines the TST. The HST in the proximal part of the foreland basin is defined by thick-bedded upper offshore, nearshore, and tidal sandstones.

which have estimated durations of 41 k.y. (Kamp and Naish, 1998; Naish et al., 1998; Pillans et al., 1998). The small-scale packages in the Wanganui basin have been interpreted as sixth-order sedimentary cycles that correspond to individual 41 k.y. sea-level changes as determined by oxygen isotope variations from deep-sea cores (Pillans et al., 1998). The oxygen isotope record from the deep-sea cores is marked by variations with a period of 40–42 k.y. that have been interpreted as a product of long-term quasi-periodic variation in Earth’s orbital obliquity (e.g., Laskar, 1990; Shackleton et al., 1990; 1995b). The duration (~37.5 k.y.) of small-scale stratigraphic packages documented in the Taiwan foreland basin may be indirectly related to the orbital time series of obliquity (40–42 k.y.), but they are not a precise match.

Interpretation of Intermediate-Scale Stratigraphic Packages

The 150–1000-m-thick, unconformity-bound stratigraphic sequences that we have identi-

fied in the Pliocene-Pleistocene foreland basin deposits are well documented in both seismic and outcrop data of south-central Taiwan. The duration of intermediate-scale packages ranges from ~100 to 700 k.y., on the basis of our magnetostratigraphy. The erosional unconformities that bound these packages have several hundreds meters of relief and define several periods of major valley incision in the foreland basin.

The angular unconformity between the Liuchungchi and Kanhsialiao Formations clearly has a tectonic origin. This angular unconformity (Fig. 11C) implies that older foreland basin deposits were structurally rotated ~31° and incised (or vice versa) prior to deposition of the overlying Kanhsialiao Formation. Similar progressively tilted strata have been described as growth strata in other foreland basin settings (DeCelles et al., 1991; Hoy and Ridgway, 1997; Ridgway et al., 1997; among others). The angular unconformity at the top of the Liuchungchi Formation, which we relate to near-surface thrust deformation, marked the beginning of a major increase in sediment ac-

cumulation rate in the Pliocene-Pleistocene foreland basin of south-central Taiwan (Fig. 14). At the contact between the Liuchungchi and the Kanhsialiao Formations, there was an increase in sediment accumulation and tectonic subsidence rates. Below the angular unconformity, average sediment accumulation rate was on the order of 950 m/m.y. in the foreland basin. Above the angular unconformity, average sediment accumulation rate was on the order of 1900 m/m.y. We interpret this unconformity that developed at ~1.25 Ma as representing structural uplift of the proximal margin of the foreland basin.

Other major unconformities in the Pliocene-Pleistocene deposits are high-relief disconformities with no evidence of structural rotation across the unconformity at outcrop scale. There was little change in sediment accumulation or tectonic subsidence rates across these unconformities at the resolution of our data (Fig. 14). These unconformities may reflect eustatic changes in the Pliocene-Pleistocene foreland basin with little change in tectonic

subsidence or sediment supply. To better evaluate possible eustatic controls on unconformity development, we use our magnetostratigraphy to compare timing of unconformity development with the oxygen isotope curves of Shackleton et al. (1990) in Figure 15. The oldest disconformity that we have recognized is at the contact between the Yunshuichi and Liuchungchi Formations; it may correlate with a major sea-level fall (stage 72) near the base of the Olduvai polarity epoch (Fig. 15). As discussed above, the contact between the Liuchungchi and Kanhsialiao Formations is an angular unconformity indicative of near-surface deformation. This unconformity is located near the base of the small *Gephyrocapsa* dominance subzone (1.22 Ma), on the basis of previously reported nanofossil stratigraphic data (Fig. 15; Horng, 1991). This unconformity, therefore, is roughly coeval with the sea-level fall represented by oxygen stage 36 in Figure 15. This correlation suggests that the tectonically generated unconformity between the Liuchungchi and Kanhsialiao Formations may have also been influenced by eustatic change. Two major disconformities, one near the top of the Kanhsialiao Formation and the other at the contact between the Kanhsialiao and Erhchungchi Formations were also documented in our study. Both of these disconformities are located between the Brunhes and Jaramillo polarity epochs and within the *Pseudoeumiliana lacunosa* subzone for nannoplanktonic biozones (Fig 15; Horng, 1991). Thus, they must have formed sometime between 0.99 and 0.78 Ma (Fig. 15). These disconformities may be correlative with sea-level falls represented by oxygen isotope stages 26 and 22. The youngest disconformity that we have recognized is located at the contact between the Erhchungchi and Liushuang Formations within the Brunhes polarity epoch. This disconformity may correlate with the major sea-level fall at 0.55 Ma (oxygen stage 14; Fig. 15). To definitively demonstrate a eustatic origin for high-relief disconformities documented in the Taiwan foreland basin deposits will require additional studies that recognize simultaneous sea-level falls in correlative age deposits on a global scale. Our attempt to correlate these previously unrecognized surfaces in the Pliocene-Pleistocene strata with the oxygen isotope curve is a first attempt to understand the possible controls on unconformity development in this foreland basin.

We interpret the intermediate-scale stratigraphic packages within the Pliocene-Pleistocene foreland basin deposits as representing "depositional sequences" of the sequence stratigraphy terminology. A sequence is a rela-

tively conformable succession of genetically related strata bounded by unconformities and their correlative conformities (Mitchum et al., 1977). The unconformities that define the incised-valley systems documented in our study of the Taiwan foreland basin appear similar to type 1 unconformities in the widely used Exxon model of sequence stratigraphy (e.g., Van Wagoner et al., 1988). These types of unconformities form as a result of erosion by fluvial processes during relative sea-level fall and lowstand, and they represent sequence boundaries (e.g., Posamentier and Vail, 1988). We interpret the abrupt change in lithofacies from lower offshore marine to nearshore estuarine deposits across major uncon-

formities in the Taiwan foreland basin strata as representing the transition from incision of offshore marine deposits during lowstand to filling of incised-valley systems by estuarine deposits during transgression. Similar "proximal over distal" basinward shifts in lithofacies have been documented across sequence boundaries associated with many other incised-valley deposits (e.g., Zaitlin et al., 1994). In addition, incised valley systems containing estuarine deposits overlain by marine mudstones, such as documented in our analysis, are quite common in other studied ancient incised-valley systems (e.g., Reinson et al., 1988; Pattison, 1991; Dalrymple et al., 1994; Zaitlin et al., 1994).

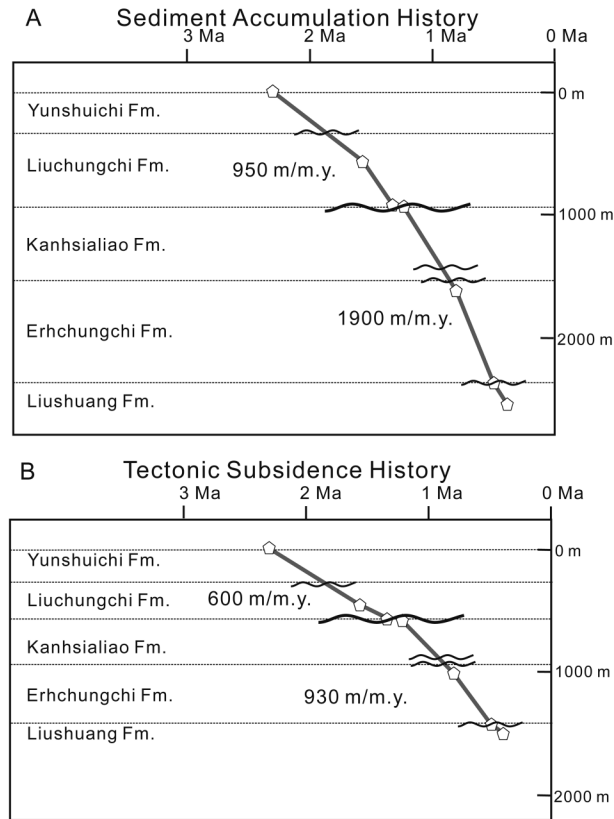
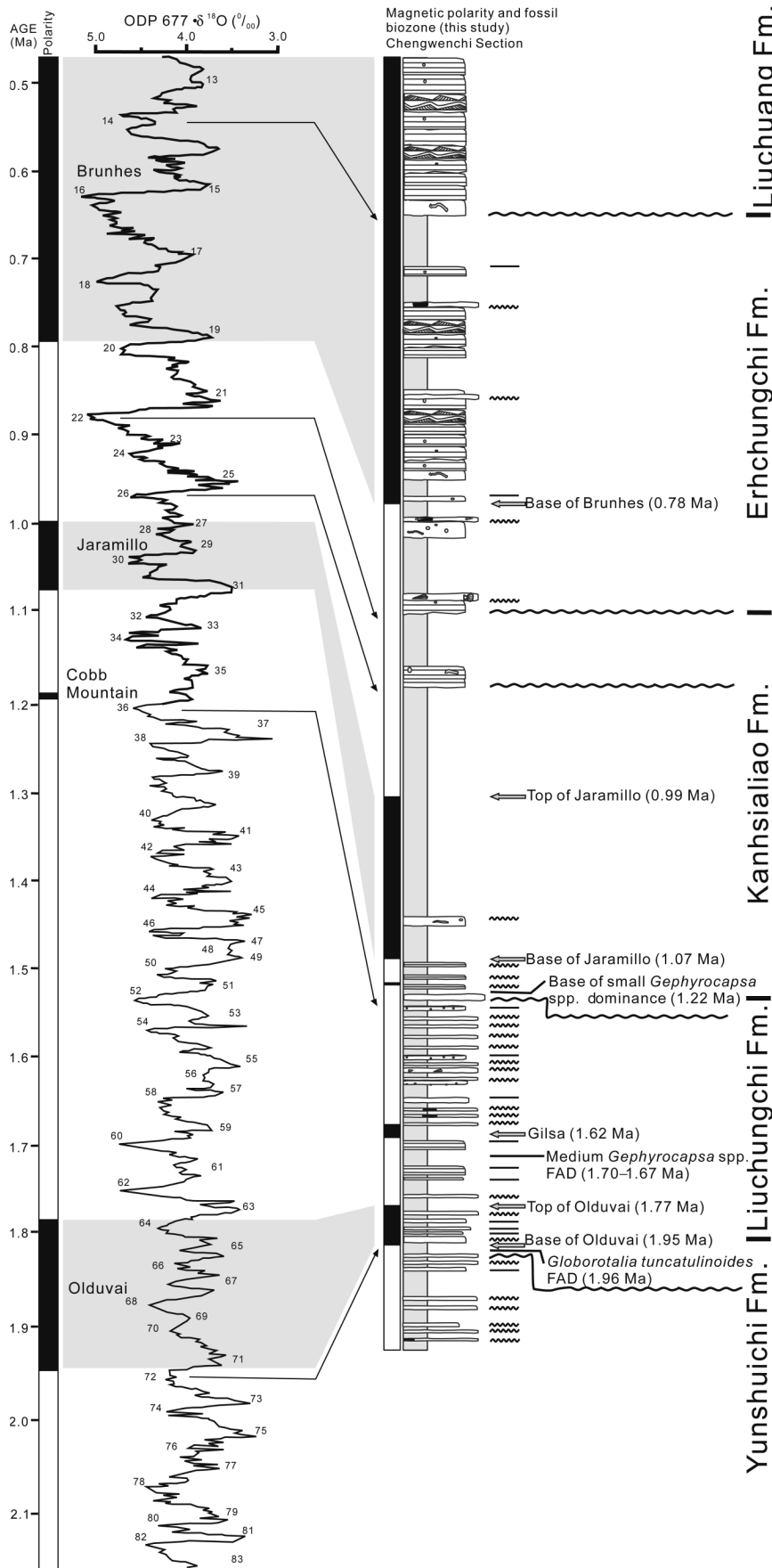


Figure 14. (A) Plot of the decompacted sediment accumulation history for the Chengwenchi measured section in south-central Taiwan (Fig. 5). Wavy lines mark positions of major unconformities that we have recognized in the foreland basin deposits. Note that sediment accumulation rate changed at the contact between the Liuchungchi and Kanhsialiao Formations. This contact is an angular unconformity at the Chengwenchi measured section (Fig. 11C). Below the angular unconformity, the average sediment accumulation rate was on the order of 950 m/m.y. Above the angular unconformity, the average sediment accumulation rate was on the order of 1900 m/m.y. Note that there was little change in sediment accumulation rate across other major unconformities. (B) Plot of the tectonic subsidence history for the Chengwenchi measured section. Wavy lines represent positions of major unconformities in the foreland basin. Note that the tectonic subsidence rate increased at the contact between the Liuchungchi and Kanhsialiao Formations. Also note that there was little change in tectonic subsidence rate across other major unconformities. Both plots were constructed using techniques discussed in van Hinte (1978) and Allen and Allen (1990).



Our analysis of intermediate-scale stratigraphic packages exposed in south-central Taiwan points out several interesting implications concerning development of this collisional marine foreland basin. Deposition in the Taiwan foreland basin appears to have been punctuated by at least five episodes of erosion and major valley incision on the basis of seismic and outcrop data. Incision produced fluvial valleys with several hundred meters of relief that allowed transport of sediment to more distal parts of the foreland basin or to depocenters outside the foreland basin system. During lowstands, sediment must have been bypassed to the mouth of the incised-valley systems where it was probably deposited in deltaic and submarine fan environments. The incision events occurred throughout the history of foreland basin development (Fig. 10), and large parts of the stratigraphic record have been eroded. The recognition of major unconformities in the Pliocene-Pleistocene foreland basin deposits also points out the potential of unexplored petroleum reservoirs associated with incised-valley deposits, and lowstand deltaic and submarine fan deposits (e.g., Howard and Whitaker, 1990; Zaitlin and Shultz, 1990; Donovan, 1995). The documentation of regional high-relief unconformities and growth structures in the Pliocene-Pleistocene foreland basin deposits of south-central Taiwan also indicates that this part of the basin was characterized by near-surface deformation and synthrusting deposition. Regional unconformities and growth structures are diagnostic features of the wedge-top depozone of foreland basin systems (DeCelles and Giles, 1996). The angular unconformity documented at the top of the Liuchungchi Formation indicates that by at least 1.25 Ma, near-surface thrust

Figure 15. Comparison of major unconformities (wavy lines on right) documented in Pliocene-Pleistocene deposits of south-central Taiwan (Chengwenchi measured section) with the oxygen isotope curve (left-center) of Shackleton et al. (1990). Shaded areas represent key paleomagnetic tie-points between our measured stratigraphic section (right) and the oxygen isotope curve. These include the Olduvai, Jaramillo, and Brunhes polarity epochs (left). Biostratigraphy for the Chengwenchi measured section is from Chen et al. (1977), Chi (1978), Chang and Chi (1983), and Horng (1991). Age ranges for biostratigraphic data are based on the international stratigraphic positions and ages defined from the time scale for Ocean Drilling Program site 677 (Shackleton et al., 1990). FAD is first-appearance biostratigraphic datum. See text for additional discussion.

faults were directly influencing deposition in this foreland basin.

Interpretation of Large-Scale Stratigraphic Packages

The large-scale stratigraphic packages documented in our measured sections from both south-central and north-central Taiwan show overall upward-coarsening and upward-shallowing trends (Figs. 5, 6). The deposits of the Pliocene-Pleistocene foreland basin record ~2.3 m.y. of deposition (Fig. 14) in an active collisional marine setting. Roughly, during the first 1 m.y. of deposition (Fig. 14; the Yunshuichi and Liuchungchi Formations), sediment accumulation rate was on the order of ~950 m/m.y. (Fig. 14). At ~1.25 Ma, sediment accumulation rate increased to ~1900 m/m.y. (Fig. 14; the Kanhsialiao, Erhchungchi, and Liushuang Formations). The sediment accumulation rate we have calculated for the Taiwan foreland basin during the past ~1.25 m.y. is much higher than the 100 to 1000 m/m.y. range documented for other foreland basins (e.g., Jordan, 1995). The extremely high sediment accumulation rate in the Taiwan foreland basin relative to other foreland basins may be related to at least two factors. First, to compare the past 1.25 m.y. of deposition in the Taiwan foreland basin to much longer-lived foreland basins may not be scale appropriate. Second, high sediment accumulation rates may be typical of collisional marine foreland basins compared to more extensively studied retroarc foreland basins and collisional nonmarine foreland basins. For example, the Apennine collisional marine foreland basin of northern Italy also appears to have had high sediment accumulation rates, up to 8 km of post-Messinian deposits (DeCelles and Giles, 1996).

SUMMARY AND CONCLUSIONS

1. Small-scale stratigraphic packages in Pliocene-Pleistocene deposits of the Taiwan foreland basin are 20 to 150 m thick and are defined by an upward-shallowing succession of lithofacies. Contacts between small-scale packages are marked by fossil-rich, marine-flooding intervals. Individual small-scale packages represent ~37.5 k.y. of deposition, on the basis of our magnetostratigraphy and are interpreted as products of eustatic sea-level change, possibly related to the orbital time series of obliquity.

2. Intermediate-scale stratigraphic packages in deposits of the Taiwan foreland basin are 150 to 1000 m thick and are bounded by unconformities that are well exposed in outcrop and can be identified on seismic profiles. The unconformities have several hundreds of meters of relief and

define five episodes of major valley incision during Pliocene-Pleistocene development of the foreland basin. One of the unconformities is locally angular; we interpret it as representing structural uplift of the proximal margin of the foreland basin at ~1.25 Ma. Across this unconformity there were marked increases in sediment accumulation and tectonic subsidence rates for the foreland basin. Other major unconformities associated with intermediate-scale stratigraphic packages are high-relief disconformities with no evidence of structural rotation across the unconformity. These unconformities may be the product of eustatic changes in the Pliocene-Pleistocene foreland basin, because there was little change in sediment accumulation and tectonic subsidence rates across the unconformities. On the basis of magnetostratigraphic and biostratigraphic data, the duration of individual intermediate-scale packages was ~100 to 700 k.y.

3. Regional high-relief unconformities and growth structures in the Pliocene-Pleistocene foreland basin deposits of south-central Taiwan suggest a well-developed wedge-top depozone in the foreland basin system.

4. The Pliocene-Pleistocene deposits of western Taiwan record ~2.3 m.y. of deposition in an active collisional marine foreland basin. Sediment accumulation rate was on the order of 950 m/m.y. during the first 1 m.y. of basin development. At ~1.25 Ma, sediment accumulation rate increased to ~1900 m/m.y. Sediment accumulation rates in the collisional marine foreland basin of Taiwan are much higher than previously published rates from more extensively studied retroarc foreland basins and nonmarine collisional foreland basins.

ACKNOWLEDGMENTS

We thank the National Science Council, Taiwan, Republic of China, for support under grants NSC-88-2116-M-002-026, NSC-89-2116-M-002-014, and NSC-90-2921-M-002-001. Ridgway also received travel support from the Purdue Research Foundation. We thank Rick Hoy, Jeff Trop, and Robin Ridgway for review of an early draft of the manuscript. Reviews by Alan Carroll, Peter DeCelles, John Geissman, and Lynn Soreghan provided many useful suggestions for improving the manuscript.

REFERENCES CITED

Allen, P.A., and Allen, J.R., 1990, Subsidence history, in Basin analysis principles and applications: Cambridge, Massachusetts, Blackwell, p. 263–281.
 Angelier, J., Barrier, E., and Chu, H.T., 1986, Plate collision and paleostress trajectories in a fold and thrust belt: The foothills of Taiwan: *Tectonophysics*, v. 125, p. 161–178.
 Berggren, W.A., Kent, D.V., Swisher, C.C., III, and Aubry, M.P., 1995, A revised Cenozoic geochronology and chronostratigraphy, in Berggren, W.A., et al., eds., *Geochronology, time scales and global stratigraphic correlations: SEPM (Society for Sedimentary Geology) Special Publication 54*, p. 129–212.

Bourgeois, J., 1980, A transgressive shelf sequence exhibiting hummocky cross stratification: The Cape Sebastian Sandstone (Upper Cretaceous), southwestern Oregon: *Journal of Sedimentary Petrology*, v. 50, p. 681–702.
 Byrne, T., and Crespi, J., 1997, Kinematics of the Taiwan arc-continent collision and implications for orogenic processes: Taiwan, National Central University, Programme and Abstracts for International Conference and Sino-American Symposium on Tectonics of East Asia, p. 38.
 Chai, B.H.T., 1972, Structural and tectonic evolution of Taiwan: *American Journal of Science*, v. 272, p. 389–422.
 Chang, S.L., and Chi, W.L., 1983, Neogene nannoplankton biostratigraphy in Taiwan and the tectonic implications: *Petroleum Geology of Taiwan*, v. 19, p. 93–147.
 Cheel, R.J., and Leckie, D.A., 1993, Hummocky cross-stratification, in Wright, V.P., ed., *Sedimentary Review*, v. 1, p. 103–122.
 Chen, P.H., Huang, T.C., Huang, C.Y., Jiang, M.J., Lo, S.I., and Kuo, C.L., 1977, Paleomagnetic and coccolith stratigraphy of Plio-Pleistocene shallow marine sediments, Chuhuankang, Miaoli: *Petroleum Geology of Taiwan*, v. 14, p. 219–239.
 Chen, W.S., Cheng, Y.M., and Huang, C.Y., 1985, Geology of the Hengchun Peninsula, southern Taiwan: *Ti-Chih*, v. 6, p. 47–74.
 Chi, W.L., 1978, The late Neogene nannobiostratigraphy in the Tainan foothills region, southern Taiwan: *Petroleum Geology of Taiwan*, v. 15, p. 89–125.
 Clifton, H.E., 1981, Progradational sequences in Miocene shoreline deposits, southeastern Caliente range, California: *Journal of Sedimentary Petrology*, v. 51, p. 165–184.
 Clifton, H.E., 1982, Estuarine deposits, in Scholle, P.A., and Spearing, D., eds., *Sandstone depositional environments*: New York, Springer-Verlag, p. 179–189.
 Covey, M., 1984, Lithofacies analysis and basin reconstruction, Plio-Pleistocene western Taiwan foredeep: *Petroleum Geology Taiwan*, v. 20, p. 53–83.
 Covey, M., 1986, The evolution of foreland basins to steady state: Evidence from the western Taiwan foreland basin: *International Association of Sedimentologists Special Publication 8*, p. 77–90.
 Dalrymple, R.W., 1992, Tidal depositional systems, in Walker, R.G., and James, N.P., eds., *Facies models: Response to sea-level change*: Waterloo, Ontario, Geological Association of Canada, p. 195–218.
 Dalrymple, R.W., Boyd, R., and Zaitlin, B.A., 1994, History of research, types and internal organization of incised-valley systems: Introduction to the volume, in Dalrymple, R.W., et al., eds., *Incised-valley systems: Origin and sedimentary sequences: SEPM (Society for Sedimentary Geology) Special Publication 51*, p. 3–10.
 DeCelles, P.A., and Giles, K.A., 1996, Foreland basin systems: *Basin Research*, v. 8, p. 105–123.
 DeCelles, P.G., Gray, M.B., Ridgway, K.D., Cole, R.B., Srivastava, P., Pequera, N., and Pivnik, D.A., 1991, Kinematic history of foreland uplift from Paleocene syn-orogenic conglomerate, Beartooth Range, Wyoming and Montana: *Geological Society of America Bulletin*, v. 103, p. 1458–1475.
 De Raaf, J.F.M., Boersma, J.R., and Van Gelder, A., 1977, Wave generated structures and sequences from a shallow marine succession, Lower Carboniferous, County Cork, Ireland: *Sedimentology*, v. 4, p. 1–52.
 Donovan, A.D., 1995, Sequence stratigraphy of Hilight Field, Powder River basin, Wyoming, U.S.A.: Unconformity control on Muddy thickness and distributions, in Van Wagoner, J.C., and Bertram, G.T., eds., *Sequence stratigraphy of foreland basin deposits: American Association of Petroleum Geologists Memoir 64*, p. 395–428.
 Gardner, M.H., Barton, M.D., Tyler, N., and Fisher, R.S., 1992, Architecture and permeability structure of fluvial-deltaic sandstones, Ferron Sandstone, east central Utah, in Flores, R.M., ed., *Mesozoic of the western interior: Tulsa, Oklahoma, Society of Economic Paleontologists and Mineralogists Guidebook*, p. 5–21.
 Hayes, J.D., Imbrie, J., and Shackleton, N.J., 1976, Variations in the earth's orbit: Pacemaker of the ice ages: *Science*, v. 194, p. 1121–1132.
 Ho, C.S., 1976, Foothills tectonics of Taiwan: *Geological Survey of Taiwan Bulletin*, v. 25, p. 9–28.

- Ho, C.S., 1982, Tectonic evolution of Taiwan: Explanatory text for the tectonic map of Taiwan: Taipei, Taiwan, Ministry of Economic Affairs, 126 p.
- Ho, C.S., 1986, A synthesis of the geologic evolution of Taiwan: *Tectonophysics*, v. 125, p. 1–16.
- Ho, C.S., 1988, An introduction to the geology of Taiwan—Explanatory text of the geologic map of Taiwan: Taipei, Taiwan, Ministry of Economic Affairs, 192 p.
- Hong, C.S., 1991, Study of magnetic minerals and magnetostratigraphy of the Tsengwenchi and Erhjenchi sections, southwestern Taiwan [Ph.D. thesis]: Taipei, National Taiwan University, 161 p. (in Chinese).
- Howard, R.H., and Whitaker, S.T., 1990, Fluvial-estuarine valley fill at the Mississippian-Pennsylvanian unconformity, Main Consolidated Field, Illinois, in Barwis, J.H., et al., eds., *Sandstone petroleum reservoirs*: New York, Springer-Verlag, p. 319–341.
- Hoy, R.G., and Ridgway, K.D., 1997, Structural and sedimentologic development of footwall growth synclines along an intraforeland uplift, east-central Bighorn Mountains, Wyoming: *Geological Society of America Bulletin*, v. 109, p. 495–523.
- Hsieh, S.L., 1990, Fission-track dating of zircons from several east-west sections of Taiwan Island [M.S. thesis]: Taipei, National Taiwan University, 134 p. (in Chinese).
- Hung, J.H., and Wiltshko, D.V., 1993, Structure and kinematics of arcuate thrust faults in the Miaoli-Cholan area of western Taiwan: *Petroleum Geology of Taiwan*, v. 28, p. 59–96.
- Hunt, D., and Tucker, M.E., 1992, Stranded parasequences and forced regressive wedge: Deposition during base level fall: *Sedimentary Geology*, v. 81, p. 1–9.
- Johnson, H.D., and Levell, B.K., 1995, Sedimentology of a transgressive, estuarine sand complex: The Lower Cretaceous Woburn Sands (Lower Greensand), southern England, in Plint, A.G., ed., *Sedimentary facies analysis*: International Association of Sedimentologists Special Publication 22, p. 17–46.
- Jordan, T.E., 1995, Retroarc foreland and related basins, in Busby, C.J., and Ingersoll, R.V., eds., *Tectonics of sedimentary basins*: Cambridge, Massachusetts, Blackwell, p. 331–362.
- Kamp, P.J.J., and Naish, T., 1998, Forward modeling of the sequence stratigraphic architecture of shelf cyclothem: Application to Late Pliocene sequences, Wanganui basin (New Zealand): *Sedimentary Geology*, v. 116, p. 57–80.
- Kirschvink, J.L., 1980, The least-squares line and plane and the analysis of paleomagnetic data: *Royal Astronomical Society Geophysical Journal*, v. 62, p. 699–718.
- Lacombe, O., Mouthereau, F., Deffontaines, B., Angelier, J., Chu, H.T., and Lee, C.T., 1999, Geometry and Quaternary kinematics of fold-and-thrust units of southwestern Taiwan: *Tectonics*, v. 18, p. 1198–1223.
- Laskar, J., 1990, The chaotic motion of the solar system: A numerical estimate of the size of the chaotic zones: *Icarus*, v. 88, p. 266–291.
- Leckie, D., 1986, Rates, controls, and sand-body geometries of transgressive-regressive packages: Cretaceous Moosebar and Gates Formations, British Columbia: *American Association of Petroleum Geologists Bulletin*, v. 70, p. 516–535.
- Leckie, D.A., and Krystinick, L.F., 1989, Is there evidence for geostrophic currents preserved in the sedimentary record of inner to middle-shelf deposits?: *Journal of Sedimentary Petrology*, v. 59, p. 862–870.
- Leckie, D.A., and Walker, R.G., 1982, Storm- and tide-dominated shorelines in Cretaceous Moosebar–Lower Gates interval outcrop equivalents of deep basin gas trap in western Canada: *American Association of Petroleum Geologists Bulletin*, v. 66, p. 138–157.
- Lee, J.C., Lu, C.Y., Chu, H.T., Delraille, B., Angelier, J., and Deffontaines, B., 1996, Active deformation and paleostress analysis in the Pakua Anticline area of western Taiwan: *Terrestrial, Atmospheric and Oceanic Sciences*, v. 4, p. 431–446.
- Martini, E., 1971, Standard Tertiary and Quaternary calcareous nanoplankton zonation, in Farinacci, A., ed., *Proceedings of Second Planktonic Conference, Rome, 1970*, p. 739–785.
- McCubbin, D.G., 1982, Barrier island and strand plain facies, in Scholle, P.A., and Spearing, D., eds., *Sandstone depositional environments*: American Association of Petroleum Geologists Memoir 31, p. 247–279.
- Miall, A.D., 1977, A review of the braided-river depositional environment: *Earth-Science Reviews*, v. 13, p. 1–62.
- Miall, A.D., 1995, Collision-related foreland basins, in Busby, C.J., and Ingersoll, R.V., eds., *Tectonics of sedimentary basins*: Cambridge, Massachusetts, Blackwell, p. 393–424.
- Mitchum, R.M., Jr., Vail, P.R., and Thompson, S., III, 1977, Seismic stratigraphy and global changes of sea level, part 2: The depositional sequence as a basic unit for stratigraphic analysis: *American Association of Petroleum Geologists Memoir* 26, p. 53–62.
- Mouthereau, F., Lacombe, O., Deffontaines, B., Angelier, J., Chu, H.T., and Lee, C.T., 1999, Quaternary transfer faulting and belt front deformation at Pakuashan (western Taiwan): *Tectonics*, v. 18, p. 215–230.
- Naish, T.R., and Kamp, P.J.J., 1997, Sequence stratigraphy of 6th order (41 K.y.) Plio-Pleistocene cyclothem, Wanganui basin, New Zealand: A case for the regressive systems tract: *Geological Society of America Bulletin*, v. 109, p. 978–999.
- Naish, T.R., Abbott, S.T., Alloway, B.V., Beu, A.G., Carter, R.M., Edwards, A.R., Journeaux, T.D., Kamp, P.J.J., Pillans, B.J., Saul, G., and Woolfe, K.J., 1998, Astronomical calibration of a Southern Hemisphere Plio-Pleistocene reference section, Wanganui basin, New Zealand: *Quaternary Science Review*, v. 17, p. 695–710.
- Pattison, S.A., 1991, Sundance and Edson valley fill deposits, in Leckie, D.A., et al., eds., 1991 NUNA Conference on High Resolution Sequence Stratigraphy, program, proceedings, and guidebook: Calgary, Alberta, Geological Association of Canada, p. 44–46.
- Pillans, B., Chappell, J., and Naish, T.R., 1998, A review of the Milankovitch climatic beat: Template for Plio-Pleistocene sea-level changes and sequence stratigraphy: *Sedimentary Geology*, v. 122, p. 5–21.
- Plint, A.G., 1988, Sharp-based shoreface sequences and “off-shore bars” in the Cardium Formation of Alberta: Their relationship to relative changes in sea level, in Wilgus, C.K., et al., eds., *Sea-level changes: An integrated approach*: Society of Economic Paleontologists and Mineralogists Special Publication 42, p. 357–370.
- Plint, A.G., Eyles, N., Eyles, C.H., and Walker, R.G., 1992, Control of sea level change, in Walker, R.G., and James, N.P., eds., *Facies models: Response to sea level change*: Waterloo, Ontario, Geological Association of Canada, p. 15–25.
- Posamentier, H.W., and Vail, P.R., 1988, Eustatic controls on clastic deposition II—Sequence and systems tract models, in Wilgus, C.K., et al., eds., *Sea-level changes: An integrated approach*: Society of Economic Paleontologists and Mineralogists Special Publication 42, p. 125–154.
- Posamentier, H.W., Allen, G.P., James, D.P., and Tesson, M., 1992, Forced regressions in a sequence stratigraphic framework: Concepts, examples, and exploration significance: *American Association of Petroleum Geologists Bulletin*, v. 76, p. 1687–1709.
- Prave, A.R., Duke, W.L., and Slattery, W., 1996, A depositional model for storm- and tide-influenced prograding siliciclastic shorelines from the Middle Devonian of the central Appalachian foreland basin, USA: *Sedimentology*, v. 43, p. 611–629.
- Reinson, G.E., Clark, J.E., and Foscolos, A.E., 1988, Reservoir geology of Crystal Viking field, Lower Cretaceous estuarine tidal channel-bay complex, south-central Alberta: *American Association of Petroleum Geologists Bulletin*, v. 72, p. 1270–1294.
- Revelle, R.R., 1990, Overview and recommendations, in Geophysics Study Committee, National Research Council, *Sea-level changes*: Washington, D.C., National Academy Press, p. 3–34.
- Ridgway, K.D., and DeCelles, P.G., 1993, Stream-dominated alluvial fan and lacustrine depositional systems in Cenozoic strike-slip basins, Denali fault system, Yukon Territory, Canada: *Sedimentology*, v. 40, p. 645–666.
- Ridgway, K.D., Trop, J.M., and Sweet, A.R., 1997, Thrust-basin formation along a suture zone, Cantwell basin, Alaska Range: Implications for development of the Denali fault system: *Geological Society of America Bulletin*, v. 109, p. 505–523.
- Rossetti, D.F., 1997, Internal architecture of mixed tide- and storm-influenced deposits: An example from the Alcântara Formation, northern Brazil: *Sedimentary Geology*, v. 114, p. 163–188.
- Shackleton, N.J., Berger, A., and Peltier, W.R., 1990, An alternative astronomical calibration of the lower Pleistocene timescale based on ODP Site 677: *Royal Society of Edinburgh Transactions*, v. 81, p. 251–261.
- Shackleton, N.J., Crowhurst, S., Hagelberg, T., Pisias, N., and Schneider, D.A., 1995a, A new late Neogene timescale: Application to Leg 138 sites, in Pisias, N., Mayer, L., Janacek, T., et al., *Proceedings of the Ocean Drilling Program, Volume 138: College Station, Texas, Ocean Drilling Program*, p. 73–101.
- Shackleton, N.J., Hall, M.A., and Pate, D., 1995b, Pliocene stable isotope stratigraphy of ODP site 846, in Pisias, N., Mayer, L., Janacek, T., et al., *Proceedings of the Ocean Drilling Program, Volume 138: College Station, Texas, Ocean Drilling Program*, p. 337–355.
- Sung, Q.C., and Wang, Y., 1985, Petrofacies of Miocene sediments in the Hengchun Peninsula and its tectonic implication: *Geological Society of China Proceedings*, v. 28, p. 23–44.
- Suppe, J., 1980, Imbricate structure of Western Foothills belt, south-central Taiwan: *Petroleum Geology of Taiwan*, v. 17, p. 1–16.
- Suppe, J., 1981, Mechanics of mountain building and metamorphism in Taiwan: *Geological Society of China Memoir* 4, p. 67–89.
- Suppe, J., 1988, Tectonics of arc-continent collision on both sides of the South China Sea: Taiwan and Mindoro: *Acta Geologica Taiwanica*, v. 25, p. 205–224.
- Swift, D.J.P., Hudelson, P.M., Brenner, R.L., and Thompson, P., 1987, Shelf construction in a foreland basin: Storm beds, shelf sandbodies, and shelf-slope depositional sequences in the Upper Cretaceous Mesaverde Group, Book Cliffs, Utah: *Sedimentology*, v. 34, p. 423–457.
- Teng, L.S., 1987, Stratigraphic records of the Cenozoic Penlai Orogeny of Taiwan: *Acta Geologica Taiwanica*, v. 25, p. 205–224.
- Teng, L.S., 1990, Geotectonic evolution of late Cenozoic arc-continent collision in Taiwan: *Tectonophysics*, v. 183, p. 57–76.
- van Hinte, J.E., 1978, Geohistory analysis—Application of micropaleontology in exploration geology: *American Association of Petroleum Geologists Bulletin*, v. 62, p. 201–222.
- Van Wagoner, J.C., Posamentier, H.W., Mitchum, R.M., Vail, P.R., Sarg, J.F., Loutit, T.S., and Hardenbol, J., 1988, An overview of the fundamentals of sequence stratigraphy and key definitions, in Wilgus, C.K., et al., eds., *Sea-level changes: An integrated approach*: Society of Economic Paleontologists and Mineralogists Special Publication 42, p. 39–45.
- Vera, J.A., and Molina, J.M., 1998, Shallowing-upward cycles in pelagic troughs (Upper Jurassic, Subbetic, southern Spain): *Sedimentary Geology*, v. 119, p. 103–121.
- Zaitlin, B.A., and Shultz, B.C., 1990, Wave-influenced estuarine sandbody: The Senlac Heavy Oil Pool, Saskatchewan, in Barwis, J.H., et al., eds., *Sandstone petroleum reservoirs*: New York, Springer-Verlag, p. 363–387.
- Zaitlin, B.A., Dalrymple, R.W., and Boyd, R., 1994, The stratigraphic organization of incised-valley systems associated with relative sea-level change, in Dalrymple, R.W., et al., eds., *Incised-valley systems: Origin and sedimentary sequences*: SEPM (Society for Sedimentary Geology) Special Publication 51, p. 45–60.

MANUSCRIPT RECEIVED BY THE SOCIETY APRIL 21, 2000
 REVISED MANUSCRIPT RECEIVED FEBRUARY 7, 2001
 MANUSCRIPT ACCEPTED MARCH 6, 2001

Printed in the USA